Check for updates

ORIGINAL ARTICLE

Deciphering the molecular mechanism of FLT3 resistance mutations

Panagiota S. Georgoulia[1†] | Sinisa Bjelic[1] | Ran Friedman[1*]

[1]Department of Chemistry and Biomedical Sciences, Linnæus Univerasity, Kalmar, SE-391 82, Sweden

[†]Present address: Department of Chemistry & Molecular Biology, University of Gothenburg, Gothenburg, SE-405 30, Sweden

[*]Corresponding author: Ran Friedman, ran.friedman@lnu.se

FMS-like tyrosine kinase 3 (FLT3) has been found to be mutated in ~30% of acute myeloid leukaemia (AML) patients. Small-molecule inhibitors targeting FLT3 that are currently approved or still undergoing clinical trials, are subject to drug resistance due to FLT3 mutations. How these mutations lead to drug resistance is hitherto poorly understood. Herein, we studied the molecular mechanism of the drug resistance mutations D835N, Y842S and M664I which confer resistance against the most advanced inhibitors, quizartinib and PLX3397 (pexidartinib), using enzyme kinetics and computer simulations. In vitro kinase assays were performed to measure the comparative catalytic activity of the native protein and the mutants, using a bacterial expression system developed to this aim. Our results reveal that the differential drug sensitivity profiles can be rationalised by the dynamics of the protein-drug interactions and perturbation of the intra-protein contacts upon mutations. Drug binding induced a single conformation in the native protein, whereas multiple conformations were observed otherwise (in the mutants or in the absence of drugs). The end-point kinetics measurements indicated that the three resistant mutants conferred catalytic activity that is at least as high as that of the reference without such mutations. Overall, our calculations and measurements suggest that the structural dynamics of the drug resistant mutants that affect the active

Accepted Article

This article has been accepted for publication and undergone full peer review but has not been through the copyediting, typesetting, pagination and proofreading process, which may lead to differences between this version and the Version of Record. Please cite this article as doi: 10.1111/FEBS.15209

This article is protected by copyright. All rights reserved

state, and the increased conformational freedom of the remaining inactive drug-bound population are the two major factors that contribute to drug resistance in FLT3 harbouring cancer cells. Our results explain the mechanism of drug resistance mutations and can aid to the design of more effective tyrosine kinase inhibitors.

Accepted Article

This article is protected by copyright. All rights reserved.

Running Title

Deciphering FLT3 drug resistance mechanism

Keywords

FLT3, leukaemia, kinase inhibitors, molecular dynamics, enzyme kinetics

Abbreviations

Abl1 Abelson murine leukaemia viral oncogene homologue 1
AML Acute myeloid leukaemia
B-ALL B-lineage (precursor-B) acute lymphoblastic leukaemia
CML chronic myeloid leukaemia
FL FLT3-ligand
FLT3 FMS-like tyrosine kinase 3
IDT Integrated DNA Technologies
ITD internal tandem duplication
IRTK insulin receptor tyrosine kinase
JM juxtamembrane
KD Kinase domain
MBP myelin basic protein
MD Molecular dynamics
MSA multiple sequence alignment
PCA Principle component analysis
PDB Protein Data Bank
PDGF platelet-derived growth factor
PSSM position specific scoring matrix
RTK receptor tyrosine kinase
TKI tyrosine kinase inhibitor
UPGMA unweighted pair group method with arithmetic mean

Introduction

FMS-like tyrosine kinase 3 (FLT3) is a class III receptor tyrosine kinase (RTK) of the platelet-derived growth factor (PDGF) receptor family. The enzyme is mainly involved in the regulation of haematopoiesis. FLT3 is normally expressed on the cell surface of haematopoietic early progenitor cells [1]. Under physiological conditions, it is activated by the binding of the cytokine FLT3-ligand (FL) on the receptor's extracellular domain. This in turn induces homodimerisation and consequent autophosphorylation of the enzyme [2]. The activated intracellular kinase domain (KD) phosphorylates and activates effector molecules of signal transduction pathways that control processes such as differentiation, proliferation and apoptosis of haematopoietic, dendritic and natural killer cells in the bone marrow [3]. The constitutive activation of FLT3 has been linked with the pathogenesis of leukaemia, in particular acute myeloid

This article is protected by copyright. All rights reserved.

Accepted Article

leukaemia (AML) and in some cases in B-lineage (precursor-B) acute lymphoblastic leukaemia (B-ALL), T-cell ALL and in lymphoid or mixed blast crisis chronic myeloid leukaemia (CML) [4–7].

More than 30% of AML patients have been found to carry gain-of-function mutations in the FLT3 gene [8, 9]. These can be in-frame internal tandem duplications (ITD) within the juxtamebrane region (JM) [10, 11], which presumably disrupt its autoinhibition potency on the KD [12, 13] and/or activating point-mutations within the KD [14–17], most often in the activation loop region (D835H/N/Y/F/V/E/G/A and Y842S/C/H, Figure 1A). The presence of these mutations in patients is linked with poor prognosis [18–22]. Thus, FLT3 has been recognised as a therapeutic target for selective and specific small-molecule tyrosine kinase inhibitors (TKIs) [23–26]. There is a growing arsenal of TKIs with activity against FLT3 that are currently undergoing clinical trials [27–32]. These include lestaurtinib (CEP-701), ponatinib (AP24534), tandutinib (MLN518), sunitinib (SU11248), sorafenib (DB00398), midostaurin (PKC412), KW2449, crenolanib (CP-868596), gilteritinib (ASP2215), quizartinib (AC220) and PLX3397 (pexidartinib). The latter two (Figure 1B) are specific FLT3 type II inhibitors, and are the subject of the current investigation. Type II inhibitors are generally more specific, targeting a particular inactive kinase conformation. This is in contrast to type I inhibitors (e.g., crenolanib) that bind to the highly conserved active kinase state, and therefore usually inhibit multiple kinase targets.

The major impediment of targeted cancer therapy is acquired clinical drug resistance [33], with TKIs displaying variant but sometimes non-overlapping resistance profiles [34–36]. Pre-existing or acquired mutations is a major TKI-escape mechanism and one of the main reasons for failure of FLT3 inhibitors [15, 16, 35, 37–44]. Quizartinib (AC220), Figure 1B, was the first drug candidate specifically designed for FLT3 that showed selectivity and potency [45, 46]. Unfortunately, quizartinib-resistant mutations in the KD (N676D, F691L/I, G697R, D835Y/V/F, Y842C/H) emerged upon treatment [42, 47]. Other drugs with activity against FLT3, such as sorafenib, are also ineffective against these mutations. Midostaurin is sensitive to KD mutations D835Y, I836del and I836M+R [15], crenolanib is effective against D835 mutants but sensitive to the gatekeeper F691L mutant [48]. Ponatinib, that is the only approved drug with activity against the notorious gatekeeper T315I mutation in Bcr-Abl, is sensitive to FLT3-F691L, as well as to KD mutations at sites Asp^{835}, Asp^{839} and Tyr^{842} [49]. PLX3397 is the only inhibitor known to date with activity against the gatekeeper F691L mutant of FLT3 (Figure 1B), but it is vulnerable to a number of other KD mutations [50].

Due to the importance of drug resistance mutations on the prognosis of patients that harbour them, it is pivotal to understand the molecular mechanism by which they cause drug resistance. This can also be useful for the design of better inhibitors or for prediction of resistance during the development of new TKIs. Mutations at sites D835 and Y842 in the activation loop and M664 in the αC-helix (Figure 1A), although not in vicinity with the drug, are the most often encountered drug resistance mutations for both quizartinib and PLX3397. Based on the frequency of occurrence and the effect on FLT3 autophosphorylation and downstream signalling [50] we chose to investigate the influence of the mutations M664I, D835N and Y842S on the structure and function of FLT3-KD. To this end, we performed a set of fully atomistic unbiased molecular dynamics simulations of the native FLT3-KD, FLT3-KD-M664I, FLT3-KD-D835N and FLT3-KD-Y842S in the inactive conformation in the absence and presence of quizartinib and PLX3397, as well as in the active conformation (Figure 1A). Whereas it is desired to study the kinetics of the pure protein experimentally, this is seldom done because FLT3 is difficult to express in bacterial cells; expression in insect or mammalian cells is laborious, expensive and time-consuming, which often make it formidable to produce sufficient amount of pure proteins as required for enzyme kinetic studies. To overcome this problem we devised a bacterial expression and purification scheme for FLT3-KD, suggesting a designed variant of FLT3-KD and carried out end point kinetics for the enzyme and the drug resistant mutants in order to study in vitro the effect of the mutations on the catalytic activity of the KD. Molecular dynamics simulations of the designed FLT3-KD were performed to investigate structural effects on the kinase inactive and active conformation. Our results support that the drug-resistant mutants of FLT3-KD are highly active due to a significantly enhanced autophosphorylation activity and any drug-bound inactive molecules are

This article is protected by copyright. All rights reserved.

Accepted Article

characterised by increased conformational freedom leading altogether to ineffective inhibition. Detailed analysis of the intra-protein contacts provided further insights into sites on the KD that emerge as hotspots for the development of drug resistance mutation sites.

Results and Discussion

Kinases, including FLT3, can adopt multiple conformations [51], some of which are catalytically operative (active state) and some are not (inactive state). The relative population of the active versus inactive state in the conformational ensemble of the KDs is the major determinant of the overall kinase activity [52]. The binding of a molecule such as a ligand, substrate or ATP can shift this equilibrium to favour either of these states. In addition, phosphorylation generally stabilises the active state and dephosphorylation shifts the equilibrium towards the inactive state. Hence, the primary mechanism of constitutive kinase activation has been suggested to be the shifting of this equilibrium towards the active state [53]. Mutations in the activation loop of the KDs often disrupt essential interactions that destabilise the inactive and energetically favour the active conformation of the activation loop, which in turn leads to a higher occupancy of the active state [43, 54–57]. For instance, mutations within the activation loop, such as H396P of Abl1 [58] and D816H/V of KIT [54] have been shown to drive the active conformation thus abolishing the inhibition by the type II inhibitor imatinib. Moreover, mutations in the activation loop of RTKs have been connected with an enhanced downstream signaling cascade, which were therefore assumed to stabilise the active conformation ("activating mutations") [14, 15, 17, 20, 21, 26, 40, 41, 50, 59].

In order to decipher the molecular mechanism of action for commonly occurring FLT3-KD drug resistance mutations we performed a set of molecular dynamics simulations. To further examine the effect of the same mutations on catalysis, we performed in vitro kinase assays of the recombinant KD of native and mutants. To this end, we developed a bacterial expression and purification scheme that enabled the fast and inexpensive production of large amounts of a pure designed variant of FLT3-KD, allowing the simultaneous and parallel study of drug-resistant mutations that often result in proteins that are toxic for the cells or have reduced solubility.

The dynamics of the protein-drug interactions explains the different sensitivity profiles of quizartinib and PLX3397

An examination of the interactions between the protein and the drugs over the simulation time revealed that neither of the drugs dissociated as there were protein-drug contacts that remained stable and present throughout the simulation time (Figure 2A, dark blue). However, a distinct interaction profile was observed for each drug as well as a significant variability which was induced by mutations that reside far from the drug binding pocket (Figures 2A, 3). PLX3397 interacted with the gatekeeper F691 and the neighbouring residues (Figure 2B). These interactions were persistent throughout the simulations (Figure 2A, dark blue area in the plot). This, in combination with the drug's smaller size (it lacks the morpholino-ethoxy group) accounts for the smaller influence of the F691L mutation on PLX3397 compared to quizartinib, where these contacts were infrequent or absent. The absence of any interaction in the adjacent region (Figure 2A, white area in the plot) is due to the fact that PLX3397 has a chloropyridine-pyrrole group instead of a imidazobenzothiazol. The imidazobenzothiazol of quizartinib interacts with residue G697 and to a lesser extent with its neighbours (Figure 2A, B). This explains the emergence of the resistance mutation G697R for quizartinib but not PLX3397 [47].

This article is protected by copyright. All rights reserved.

Accepted Article

Both drugs stabilise a single conformational ensemble in the native protein, but not in the resistant mutants

In order to examine if the presence of either mutation affects the conformational equilibrium of inactive and active states we performed a principle component analysis (PCA)-based cluster analysis of the conformations observed during each cumulative 1μs trajectory (Figures 4, 5). In all cases, the inactive drug-free state could adopt several different conformations as represented by the higher number of conformational clusters, with the occupancy of the dominant cluster ranging between 36–50%. The active state on the other hand was associated with fewer accessible conformations as interpreted by the presence of one dominant cluster (84%–94% of the total cluster-assigned frames in all sets of simulations). The presence of either of the mutations does not seem to affect this balance, with an additional yet minor stabilising effect towards the main cluster of conformations (84% for the native compared to over 90% for the mutants). Binding of the drug in the inactive state of the native KD leads to a higher dominance of the main conformational cluster which is adopted by 82% or 94% of the ensemble's clustered configurations for quizartinib and PLX3397, respectively. This effect seems to be perturbed by the presence of the resistance mutations studied here. In all combinations of mutations/drugs we observed a larger number of clusters and smaller amount of individual configurations that comprise the main cluster (25%–69%) of the drug-bound inactive conformation. This may indicate that the low-energy conformation as seen in the crystal structure is destabilised by the mutations to some extent.

Quizartinib and PLX3397 perturb intra-protein contacts, and do so in different ways

In order to examine the source of the conformational perturbation induced by the presence of either drug or resistance mutations, we calculated the protein contact maps over the course of each simulation. These frequency-contact maps reveal some interesting aspects upon one-to-one comparison of the different simulation systems (Figures 6, 7). The total number of contacts remained similar on average in the various systems but in some cases we could identify hotspots on the protein structure where many contacts were rearranged, the most representative examples of which are shown in Figure 6.

The effects of the drugs on the intra-protein contacts network are shown in the upper row of Figure 6 (panels A,B,C). The presence of PLX3397 (panel A) disrupted some interactions between the activation loop, the P-loop and the αC-helix (red shaded lines in Figure 6A represent contacts that were present in the trajectory when the protein was simulated in the absence of PLX3397, but were not observed with the inhibitor). Instead, some new contacts were formed in the C-lobe in the vicinity of the catalytic loop (blue-shaded lines in the same figure). The presence of quizartinib (panel B) seems to have disrupted similar contacts (red shaded lines in Figure 6B) but the newly formed contacts were located in the N-lobe area and more specifically in the P-loop/αC-helix interface. This is more evident in the direct comparison between the two drug-bound systems (panel C). These differences can be rationalised by the fact that quizartinib is a larger molecule than PLX3397 and in the crystal structure occupies a site termed the "specificity pocket" adjacent to the ATP binding site towards the αC-helix [59].

Importantly, analysis of the variation of the contact maps can be used to suggest particular areas on the KD that might be sensitive for development of drug resistance mutations where a significant degree of perturbation is observed. For example, since quizartinib perturbs contacts in the P-loop/αC-helix interface (panels B, C) individual mutations in this area may lead to resistance against the drug. Indeed, all documented quizartinib-resistance mutations concern residues that span the same area (Figure 6B). In contrast, in the presence of PLX3397 the perturbation is much weaker

This article is protected by copyright. All rights reserved.

Accepted Article

(in the order of only 20% difference), in which case it is difficult to predict if mutations in this area are likely to lead to resistance. PLX3397 has a more variant sensitivity profile, with mutations arising in the αC-helix and the activation loop (Figure 6A), covering more extensive interaction areas. In this case, the resistance mutations act allosterically and alternative kinase conformations should be explored to understand their mechanism, as discussed below.

The drug resistance mutations interfere with intra-protein contacts in the active conformation

For the mutation sites D835 and Y842 in the activation loop and M664 at the αC-helix, the implication in drug resistance could not be deduced from a comparison of the simulations in the inactive conformation in the absence and presence of the drugs. Therefore, a comparison of the effect of each mutation on the active and inactive conformations was performed. In all three cases, the effect of each mutation on the inactive conformation was negligible since the initial native contacts were highly preserved (Figure 7, first row). The case of Y842S might seem contradictory, but a closer examination revealed that the contact rearrangement concerned only a couple of contact pairs in the activation loop which did not have a significant impact on the loop arrangement. When modelling each mutation on the active conformation (Figure 7, second row) we observed a quite noticeable difference. M664I showed the most striking effect (Figure 6D), with the activation loop forming many new contacts with the αC-helix and the C-lobe, contributing to its stabilisation in the active configuration. The same trend in the active conformation was observed for the other two mutations, D835N and Y842S, with many new contacts observed in the C-lobe and between the activation loop and the C-lobe. That the interactions when the activation loop is in the active configuration are strengthened in the presence of the mutations will make the transition of the activation loop to the inactive configuration less probable compared to the native protein. This in turn could lead to a more populated active state, compared to the inactive one. The relative stability of the active conformation might then be affected by the nature of the mutation itself. Especially in the case of D835, the most often and variably mutated residue (D835H/N/Y/F/V/E/G/A), each of these different mutations would lead to a different contacts pattern, providing an explanation to their differential resistance profiling to drugs [43].

When it comes to a combination of the mutations/drugs in the inactive conformation (Figure 7, third and fourth row), the observed differences in the protein's contacts network were more pronounced owing to the presence of the drug rather than the mutation itself. This can be easily concluded by observing the high similarity of the difference maps for the drugs in the native sequence (blue-shaded lines in Figure 6A, B) to the corresponding ones in the mutants (red-shaded lines in Figure 7, third and fourth row, respectively). The imposition of either mutation in the inactive conformation when the drug is present seems to be negligible. An exception is the case of Y842S mutation with quizartinib, where there is a higher level of contact rearrangement especially in the interface of P-loop with the drug binding pocket. This was not observed though in the combination of Y842S mutation with PLX3397. The Y842S mutant is resistant to PLX3397 but not to quizartinib [50] and it is likely that the rearrangement of contacts here is one of the reasons for this.

FLT3-KD drug resistance mutations appear to be at least as active as the native protein

The effect of the occurrence of drug resistance mutations on the downstream signaling in cells [50] together with our calculations that suggest that the same mutations seem to have a larger effect on the active conformation (Results

This article is protected by copyright. All rights reserved.

Accepted Article

and Discussion, subsections "Both drugs stabilise a single conformational ensemble in the native protein, but not in the resistant mutants" and "The drug resistance mutations interfere with intra-protein contacts in the active conformation") prompted us to look further into determining their in vitro catalytic activity. Native FLT3-KD could not be expressed in bacterial cells, which was presumably due to instability or misfolding that was not alleviated by including a phosphatase [60] (details are provided in Experimental procedures subsection "Computational design of a soluble active FLT3-KD"). To overcome this limitation, we used a computational protocol [61] wherein surface residues where mutated based on a multiple sequence alignment (MSA) to make the protein more soluble while minimally affecting the catalytic efficiency and without interfering with the important structural features of the protein (Figure 8A). The introduced surface residue mutations made it possible to produce FLT3-KD of high purity (Figure 8B), in monomeric form (Figure 8C) and of comparable catalytic activity with the native (commercially available) enzyme (Figure 8D,E). Addition of each of the drug resistance mutations resulted in an almost two-fold increase of the enzyme's catalytic activity (relative to the designed enzyme) as judged by the reaction velocity divided by enzyme concentration (Figure 8D). Autophosphorylation was similar between the native enzyme and designed variant, whereas the activity was higher for the mutants tested (Figure 8E). Together with the conformational changes observed in the simulations, the results imply that these particular drug resistance mutations favour a conformation that promotes the enzyme's higher activation by increasing its autophosphorylation rate. We note, however, that since the autophosphorylation rate is rather similar to the rate of the reaction with the substrate, it is difficult to discern if the mutant enzymes are more biologically active based on the kinetics data.

The higher autophosphorylation potency could be due to the increased ability to bind ATP, as reported for the D161A activation loop mutant of the insulin receptor tyrosine kinase [62]. This is also supported by the lower K_M for ATP of FLT3 mutants like ITD and D835Y (1–2μM) compared to the native (5–8μM) as reported by commercial companies (ProQinase and Cell Signaling Technology). KIT drug resistant activation loop mutants also show increased affinity to ATP as expressed by the reduced K_M values determined in vitro [54]. Another possibility is that these activation loop mutations shift the conformational equilibrium towards a prone-to-autophosphorylate conformation, which is distinct from the active conformation and has the catalytic motifs aligned [63]. Similar constitutive autophosphorylation has been shown for activation loop mutants I836del and I836M/R of FLT3-KD in HEK 293 and Ba/F3 cell lines [15].

The analysis of possible autophosphorylation sites in the FLT3-KD revealed Tyr^{842} located in the activation loop as the single modifiable site. Other known phosphorylation sites for FLT3-KD that could potentially serve as autophosphorylation sites are neither present in the protein construct nor in the crystallographically determined structures used in the simulations. Calculations of the solvent-accessible area of Tyr^{842} during the course of the simulations did not reveal any statistically significant differences to support a differentially exposed residue in the simulations of the native and the mutants. The putatively phosphorylated tyrosine residue in the activation loop of homologue kinases is usually engaged, in the inactive conformation, in a hydrogen bond with a neighbouring aspartic acid that serves as the catalytic base (proton acceptor) in the phosphoryl transfer reaction. This is common in tyrosine kinases where phosphorylation of the tyrosine residue is crucial for the transition of the activation loop to the active conformation. In FLT3-KD, this pair constitutes Tyr^{842} and Asp^{811} but in the simulations of the native protein, the hydrogen bond is not persistent (calculated occupancy of 22% of the total simulation time). This is in accordance with a different mechanism observed in some kinases like KIT [64] and Abl1 [65], where phosphorylation is crucial to maintain the kinase in the active conformation and transmit the signal but is not essential for its catalytic activity. This is a characteristic feature of protein kinases that rely on autophosphorylation for activation. Indeed, phosphorylation of Tyr^{842} in FLT3 has been shown that is not important for activation but it is critical for the downstream signaling [66].

This article is protected by copyright. All rights reserved.

Conclusions

Unbiased molecular dynamics simulations of FLT3 KD were carried out for the native protein and the drug resistant mutants, M664I, D835N and Y842S, in the active and inactive states, and in the presence and absence of the drugs quizartinib and PLX3397. The calculations were used to clarify the differential drug sensitivity profiles by analysing the dynamics of the protein-drug and intra-protein interactions in the context of the mutations. Importantly, analysis of the simulations highlighted the stabilisation of a single KD conformation induced by binding of either of the two drugs, which was perturbed in the presence of each of the studied mutations. Comparative analysis of the intra-protein contacts network in the active and inactive states revealed that these particular mutations do not perturb the inactive state, which binds the drugs. Rather, they appear to drive the equilibrium towards the active conformation by strengthening the contacts that stabilise the activation loop in the active configuration making the transition to the inactive configuration less probable. In vitro kinase assay of the native (designed construct) KD and the mutants revealed that the three mutants were as active as the wild type FLT3, if not more.

It is often difficult to discern what makes certain mutants resistant against drug therapy when the mutations do not involve residues that directly interact with the drug [67]. The main outcome of the present work is that drug resistance can emerge by mutations such as M664I, D835N, Y842S by making an enzyme that is more likely to adopt an active conformation; the active state is inaccessible for binding by type II TKIs, such as quizartinib and PLX3397. In addition, the mutants may be somewhat more active. In previous work, we showed an alternative drug resistance mechanism for Abl1 kinase, wherein ponatinib-resistant compound mutations gave rise to a catalytically more efficient enzyme due to an increase in the affinity for the substrate [68]. Drug-resistant mutations seem to arise in the cell populations because they yield a fitness advantage to the mutant enzyme by making it more catalytically efficient. An increase in the catalytic efficiency due to change in the protein dynamics has also been shown for driver mutations in another oncogenic kinase [69, 70], supporting this view.

Our results contribute to the understanding of the molecular mechanism by which drug-resistant mutations drive FLT3's oncogenicity and uncontrolled signaling. More importantly, such an analysis can be utilised to predict conformational preferences for a KD in the presence of a TKI and suggest putative sites for the development of drugs that overcome resistance. This information can then be exploited in designing combinatorial schemes of clinically active inhibitors with enhanced resistance profiles. Furthermore, TKI design studies could also turn towards targeting the autophosphorylation prone transient kinase structure, as enhanced catalytic activity appears to be a general mechanism of escape from drugs. The Abl1 kinase, for example, seems to not have evolved for maximal efficiency, perhaps because these enzymes have to be tightly regulated. The same is likely true for many other kinases.

Materials and methods

Structure preparation for molecular dynamics simulations

All models of the FLT3-KD in the inactive conformation were prepared using the crystal structure in complex with quizartinib, **PDB ID 4RT7** [50]. Missing residues were built with Modeller (version 9.16) [71]. For the complex with the PLX3397 inhibitor, the structure was prepared after structural alignment of the inactive FLT3-KD with the crystal structure of FMS-KD of CSF-1-R in complex with PLX3397 (Cα-atoms RMSD: 0.87Å, sequence identity: 62%, sequence similarity: 78%, **PDB ID 4R7H** [72]), with the pose of the PLX3397 replacing quizartinib (Figure 9). Force field parameters for both drugs were generated with the SwissParam server [73]. Mutations were introduced using UCSF Chimera followed by energy minimisation [74].

In the absence of a crystallographic structure for the active conformation of FLT3-KD, a model was prepared through

This article is protected by copyright. All rights reserved.

the following procedure. A search was performed in the PDB database to select all kinases that included the DFG motif in their sequence and sorted out for the ones that had the activation loop in the configuration of the active conformation (Figure 1A). This resulted in 62 PDB files that were used to prepare a multiple sequence alignment (MSA) with ClustalW [75] and construct a UPGMA tree with MAFFT [76] (Figure 10). The 22 active kinase conformations that were the closest to FLT3-KD (red branches in Figure 10) were used as template in Modeller [71] to prepare the model of the active FLT3-KD. Mutations in the active conformation were introduced as before.

To evaluate the qualitative agreement of the dynamics of the designed FLT3-KD with these of the native protein, a model of the design was also prepared, with the 10 mutations introduced as before, in the context of the inactive and active FLT3-KD, termed design inactive and design active, respectively. The design was also modelled together with the M664I mutation in the inactive and active conformations as well, termed design M664I inactive and design M664I active.

Simulation protocol

All system preparation and simulations were performed with Gromacs (v2016.1) [77, 78]. In total, 20 systems were studied with the CHARMM27 [79, 80] force field for a cumulative time of 20 μs (1 μs each) using explicit solvent, full treatment of the electrostatics and periodic boundary conditions. To enhance sampling of the local accessible conformations we performed for each system 20 replicas of 50ns each. In brief, the protein was solvated in a cubic box of pre-equilibrated TIP3P water molecules [81] with an initial distance between the solute and the edge of the box of 1 nm along with potassium and chlorine ions to a final concentration of 100 mM to mimic experimental ionic strength conditions. The final systems comprised approximately 63000 and 58000 atoms for the inactive and active conformations, respectively. At first, systems were energy minimised for 5000 steps or more with a steepest descent algorithm until the maximal force on individual atoms was smaller than 100 KJ mol^{-1} nm^{-1}. Thereafter, a short (20 ps) run was performed with positional restraints on all protein heavy atoms and the crystallographic water molecule found in the drug-binding pocket which were subsequently released and the whole system was equilibrated for 5 ns. This was followed by the production NpT runs with the temperature (300 K) kept constant using the velocity rescaling thermostat [82] and the pressure (1 atm) controlled with Berendsen's barostat [83] during equilibration, and the Parrinello-Rahman algorithm [84] during production runs. The simulation timestep was 2 fs with van der Waals forces truncated at 1 nm with a plain cutoff and long-range electrostatics treated with the PME method [85, 86]. LINCS algorithm [87] was used to constrain bond lengths and water molecules were kept rigid through the SETTLE algorithm [88]. Trajectories were obtained by saving atomic coordinates every 10 ps.

Trajectory analysis

The programs Gromacs [77, 78], CARMA [89] and Pymol [90] together with custom scripts were used for the analyses of the trajectories and preparation of molecular graphics work. Only the production runs were used for all analyses, where the RMSD from starting structure had stabilised (simulations in the inactive conformation and active conformation had an average Cα-atoms RMSD of 1.45(± 0.17)Å and 2.13(± 0.18)Å, respectively. Dihedral PCA analysis and corresponding cluster analysis were performed with CARMA. The projection of each trajectory on the two principal components is shown in Figure 5. Clustering was performed taking into account the first five principal components. The number of clusters was chosen as to maximise the variance explained, which ranged from 0.57 to 0.81 (1.00 meaning that 100% of the data variation is explained by the clustering) and is given in the bottom right of each subfigure. For the calculation of contact maps, custom scripts were used to calculate the residue-residue contacts every

This article is protected by copyright. All rights reserved.

Accepted Article

100ps, using a Cα-Cα distance cutoff of 8Å, which were then converted to frequency contact maps over the total simulation time. The visualisation of the contacts on the protein structure was performed with Pymol using a custom modification of the bio3d R package [91].

Computational design of a soluble active FLT3-KD

The FLT3-KD was overexpressed in *E.coli* using different schemes (codon optimised gene with N-terminal His-tag or C-terminal His-tag or N-terminal His-MBP-tag, with and without the JM region) but was found consistently insoluble even when co-expressed with a phosphatase that gave satisfactory results for other tyrosine kinases [60]. When heterologous overexpression fails, it is common to resort to insect or human cell cultures. These solutions can also be troublesome as they either have prohibitively high cost or yield limited quantities, precluding biochemical and biophysical studies. Hence, the Rosetta [92] PROSS server interface [61] was used to suggest an increasing number of surface mutations that can have a solubilisation effect. This design algorithm suggests a combination of mutations based on a position specific scoring matrix (PSSM) calculated from an MSA of homologous proteins that minimise the computed energy and thus increase the predicted stability of the modelled structure. This approach was employed to a kinase for the first time but has thus far been successfully applied to a number of other enzymes, spanning from acetylcholinesterases to methytransferases [61]. To this end and after testing a number of variants, the following combination of mutations gave a soluble active designed protein: Q667H, F804S, S806N, F906Y, F912E, I920Q, S930P, N938Q, T940V, S941Q (Figure 8A). None of these mutations is important for the function of the enzyme and neither of them is documented as drug resistance mutations in the literature. We anticipate that the suggested designed active FLT3-KD that can be easily bacterially produced and purified to homogeneity (Figure 8B, C) can find broad applicability to other research groups performing FLT3-related studies.

Computational validation of the designed FLT3-KD

A set of MD simulations was performed on the designed FLT3-KD to evaluate if the designed enzyme qualitatively reflects the conformational behaviour of the native enzyme, which was indeed the case (Figure 11A). In more detail, in Figure 11A, we present the distribution of the minimum RMSD values calculated for each pair of closest structures found in the two respective native-design simulation systems. The vast majority of the conformations observed during the design simulation were very close (0.6-0.8Å RMSD values) to the ones observed during the native simulation, in both inactive and active conformations (black and brown lines, respectively). On the other hand, imposition of a drug resistance mutation, like M664I, in the background of the ten solubilising mutations of the designed enzyme, increased the conformational variation with the majority of the structures observed in the design M664I simulation being more distinct from the structures observed in the M664I simulations (1.2-1.6Å RMSD values, red and orange lines for inactive and active conformations, respectively). The same conclusion is drawn even if we compare all clustered structures observed in the native simulation over the ones observed in the design simulation (Figure 11B). This is also reflected in the dihedral PCA-based cluster analysis (Figure 11C,D). The relative distribution of the clusters and their occupancy did not change much, especially when comparing the native (native, M664I) and designed (design, design M664I) systems in the active conformation. A slightly increased variation was observed in the case of inactive conformations, which was more pronounced for the M664I system (M664I, design M664I), in accordance with the RMSD-based results. Thus, mutations seem to affect the conformational ensemble of the inactive state more than the one of the active state, a feature that becomes more pronounced for mutations that have been characterised as drug resistance mutations, like M664I, but the results were overall similar for the native and designed protein.

This article is protected by copyright. All rights reserved.

Accepted Article

Protein expression and purification

The KD domain of the FLT3 gene (residues 599-950) was synthesised by Integrated DNA Technologies (IDT, Leuven, Belgium) and cloned into pet29b+ using the NdeI and XhoI restriction sites, adding a C-terminal hexa-histidine tag. The single point mutations (M664I, D835N, Y842S) were introduced with the Kunkel mutagenesis protocol [93] using the FLT3 design gene as a template and mutagenic primers synthesised by IDT. All gene sequences were confirmed by sequencing (Eurofins Genomics, Ebersberg, Germany). The design FLT3-KD and the mutants were overexpressed in *E.coli* BL21(DE3) tuner cells together with the Yop phosphatase (a generous gift from Markus Seeliger). Cells were grown at 37 °C to an $OD_{600\,nm}$ of 0.8 and induced with 0.5 mM isopropyl-b-D-thiogalactoside for 5 h at 25 °C. Cells were harvested by centrifugation and stored at −20 °C. Pelleted cells were resuspended in lysis buffer (50 mM Hepes, pH 7.4, 500 mM NaCl, 10 mM imidazole, 20% glycerol, 1% Triton X-100, 5 mM 2-mercaptoethanol) supplemented with EDTA-free protease inhibitor cocktail (Thermo Scientific) and lysed by sonication followed by centrifugation to clear the lysate. Protein purification was carried out by Nickel affinity chromatography (HisTrap HP, GE Healthcare Life Sciences, Uppsala, Sweden) using an automated FPLC system. Eluted proteins were pooled and concentrated prior injection to a gel filtration column (Superdex 200 HR 10/30, GE Healthcare Life Sciences, Uppsala, Sweden) pre-equilibrated with GF buffer (20 mM Tris-HCl pH 8.0, 100 mM NaCl, 5% glycerol, 1 mM DTT). Peak fractions were analysed by SDS-PAGE and the ones containing pure kinase were pooled, adjusted to a final concentration of 0.1 μg/μL, aliquoted, flash-frozen in liquid nitrogen and stored at −80 °C.

In vitro kinase assay

The ADP-Glo Assay (Promega Biotech AB, Stockholm, Sweden) was used to determine the catalytic activity of the kinases, following the manufacturer's protocol. The native (commercially available) FLT3 (residues 571-993, N-terminal GST-tag, expressed in baculovirus Sf9 insect cells) was purchased from SignalChem to compare its enzymatic activity with our design. All kinases and reagents were diluted in kinase buffer (40 mM Tris pH 7.5, 20 mM MgCl2, 0.1 mg/mL BSA, 50 μM DTT). For the determination of the enzymatic parameters of the KD, 20 μL reaction mixtures were prepared using 10 ng/μL kinase, 50 μM ATP and serial two-fold dilutions of myelin based protein (MBP, SignalChem) as substrate, with 300 μM initial concentration. The same reaction set-up without the MBP substrate was used to determine the autophosphorylation activity. All reactions were carried out in triplicate for 1 h at 25 °C using opaque white flat bottom half area 96-well polystyrene assay plates (Corning). In all cases, a high autophosphorylation signal was measured, hence the K_M parameter could not be determined accurately because of the significant competition at low substrate concentrations. For the determination of the maximum velocity of the MBP phosphorylation an average of the two highest substrate concentrations was used instead. Luminescence was measured using a TECAN SPARK 10M plate reader with an integration time of 1 sec. ATP-ADP conversion curves were performed to convert relative units of luminescence to reaction velocities. Comparisons in activity values were analysed with one-way ANOVA.

Accepted Article

This article is protected by copyright. All rights reserved.

references

[1] William Matthews, Craig T Jordan, Gordon W Wiegand, Drew Pardoll, and Ihor R Lemischka. A receptor tyrosine kinase specific to hematopoietic stem and progenitor cell-enriched populations. *Cell*, 65(7):1143–1152, 1991.

[2] Stewart D Lyman. Biology of flt3 ligand and receptor. *International journal of hematology*, 62(2):63–73, 1995.

[3] T Naoe and H Kiyoi. Normal and oncogenic flt3. *Cellular and molecular life sciences: CMLS*, 61(23):2932–2938, 2004.

[4] F Birg, Marianne Courcoul, Olivier Rosnet, Florence Bardin, Marie-Josephe Pebusque, Sylvie Marchetto, Antonio Tabilio, Patrice Mannoni, and Daniel Birnbaum. Expression of the fms/kit-like gene flt3 in human acute leukemias of the myeloid and lymphoid lineages. *Blood*, 80(10):2584–2593, 1992.

[5] HG Drexler. Expression of flt3 receptor and response to flt3 ligand by leukemic cells. *Leukemia*, 10(4):588–599, 1996.

[6] Catherine E Carow, Mark Levenstein, Scott H Kaufmann, Joseph Chen, Shahina Amin, Patricia Rockwell, Larry Witte, Michael J Borowitz, Curt I Civin, and Donald Small. Expression of the hematopoietic growth factor receptor flt3 (stk-1/flk2) in human leukemias. *Blood*, 87(3):1089–1096, 1996.

[7] Kazutaka Ozeki, Hitoshi Kiyoi, Yuka Hirose, Masanori Iwai, Manabu Ninomiya, Yoshihisa Kodera, Shuichi Miyawaki, Kazutaka Kuriyama, Chihiro Shimazaki, Hideki Akiyama, Miki Nishimura, Toshiko Motoji, Katsuji Shinagawa, Akihiro Takeshita, Ryuzo Ueda, Ryuzo Ohno, Nobuhiko Emi, and Tomoki Naoe. Biologic and clinical significance of the flt3 transcript level in acute myeloid leukemia. *Blood*, 103(5):1901–1908, 2004.

[8] D Gary Gilliland and James D Griffin. The roles of flt3 in hematopoiesis and leukemia. *Blood*, 100(5):1532–1542, 2002.

[9] Derek L Stirewalt and Jerald P Radich. The role of flt3 in haematopoietic malignancies. *Nature Reviews Cancer*, 3(9):650, 2003.

[10] M Nakao, S Yokota, T Iwai, H Kaneko, S Horiike, K Kashima, Y Sonoda, T Fujimoto, and S Misawa. Internal tandem duplication of the flt3 gene found in acute myeloid leukemia. *Leukemia*, 10(12):1911–1918, 1996.

[11] H Kiyoi, T Naoe, S Yokota, M Nakao, S Minami, K Kuriyama, A Takeshita, K Saito, S Hasegawa, S Shimodaira, J Tamura, C Shimazaki, K Matsue, H Kobayashi, N Arima, R Suzuki, H Morishita, H Saito, R Ueda, and R Ohno. Internal tandem duplication of flt3 associated with leukocytosis in acute promyelocytic leukemia. *Leukemia*, 11(9):1447, 1997.

[12] H Kiyoi, M Towatari, S Yokota, M Hamaguchi, R Ohno, H Saito, and T Naoe. Internal tandem duplication of the flt3 gene is a novel modality of elongation mutation which causes constitutive activation of the product. *Leukemia*, 12(9):1333, 1998.

[13] James Griffith, James Black, Carlos Faerman, Lora Swenson, Michael Wynn, Fan Lu, Judith Lippke, and Kumkum Saxena. The structural basis for autoinhibition of flt3 by the juxtamembrane domain. *Molecular cell*, 13(2):169–178, 2004.

[14] Yukiya Yamamoto, Hitoshi Kiyoi, Yasuyuki Nakano, Ritsuro Suzuki, Yoshihisa Kodera, Shuichi Miyawaki, Norio Asou, Kazutaka Kuriyama, Fumiharu Yagasaki, Chihiro Shimazaki, Chihiro Shimazaki, Hideki Akiyama, Kenji Saito, Miki Nishimura, Toshiko Motoji, Katsuji Shinagawa, Akihiro Takeshita, Hidehiko Saito, Ryuzo Ueda, Ryuzo Ohno, and Tomoki Naoe. Activating mutation of d835 within the activation loop of flt3 in human hematologic malignancies. *Blood*, 97(8):2434–2439, 2001.

[15] Rebekka Grundler, Christian Thiede, Cornelius Miething, Christine Steudel, Christian Peschel, and Justus Duyster. Sensitivity toward tyrosine kinase inhibitors varies between different activating mutations of the flt3 receptor. *Blood*, 102(2):646–651, 2003.

[16] Jennifer J Clark, Jan Cools, David P Curley, Jin-Chen Yu, Nathalie A Lokker, Neill A Giese, and D Gary Gilliland. Variable sensitivity of flt3 activation loop mutations to the small molecule tyrosine kinase inhibitor mln518. *Blood*, 104(9):2867–2872, 2004.

Accepted Article

This article is protected by copyright. All rights reserved.

[17] Thomas Kindler, Frank Breitenbuecher, Stefan Kasper, Eli Estey, Francis Giles, Eric Feldman, Gerhard Ehninger, Gary Schiller, Virginia Klimek, Stephen D Nimer, Alois Gratwohl, Chuna Ram Choudhary, Constan Mueller-Tidow, Hubert Serve, Harald Gschaidmeier, Pamela S. Cohen, Christoph Huber, and Thomas Fischer. Identification of a novel activating mutation (y842c) within the activation loop of flt3 in patients with acute myeloid leukemia (aml). *Blood*, 105(1):335–340, 2005.

[18] FM Abu-Duhier, AC Goodeve, GA Wilson, MA Gari, IR Peake, DC Rees, EA Vandenberghe, PR Winship, and JT Reilly. Flt3 internal tandem duplication mutations in adult acute myeloid leukaemia define a high-risk group. *British journal of haematology*, 111(1):190–195, 2000.

[19] Panagiotis D Kottaridis, Rosemary E Gale, Marion E Frew, Georgina Harrison, Stephen E Langabeer, Andrea A Belton, Helen Walker, Keith Wheatley, David T Bowen, Alan K Burnett, Anthony H Goldstone, and David C Linch. The presence of a flt3 internal tandem duplication in patients with acute myeloid leukemia (aml) adds important prognostic information to cytogenetic risk group and response to the first cycle of chemotherapy: analysis of 854 patients from the united kingdom medical research council aml 10 and 12 trials. *Blood*, 98(6):1752–1759, 2001.

[20] Stefan Fröhling, Richard F Schlenk, Jochen Breitruck, Axel Benner, Sylvia Kreitmeier, Karen Tobis, Hartmut Döhner, and Konstanze Döhner. Prognostic significance of activating flt3 mutations in younger adults (16 to 60 years) with acute myeloid leukemia and normal cytogenetics: a study of the aml study group ulm. *Blood*, 100(13):4372–4380, 2002.

[21] Christian Thiede, Christine Steudel, Brigitte Mohr, Markus Schaich, Ulrike Schäkel, Uwe Platzbecker, Martin Wermke, Martin Bornhäuser, Markus Ritter, Andreas Neubauer, Gerhard Ehninger, and Thomas Illmer. Analysis of flt3-activating mutations in 979 patients with acute myelogenous leukemia: association with fab subtypes and identification of subgroups with poor prognosis: Presented in part at the 42nd annual meeting of the american society of hematology, december 1-5, 2000, san francisco, ca (abstract 2334). *Blood*, 99(12):4326–4335, 2002.

[22] M Yanada, K Matsuo, T Suzuki, H Kiyoi, and T Naoe. Prognostic significance of flt3 internal tandem duplication and tyrosine kinase domain mutations for acute myeloid leukemia: a meta-analysis. *Leukemia*, 19(8):1345, 2005.

[23] Tomoki Naoe, Hitoshi Kiyoi, Yukiya Yamamoto, Yosuke Minami, Kazuhito Yamamoto, Ryuzo Ueda, and Hidehiko Saito. Flt3 tyrosine kinase as a target molecule for selective antileukemia therapy. *Cancer chemotherapy and pharmacology*, 48(1):S27–S30, 2001.

[24] Charles L Sawyers. Finding the next gleevec: Flt3 targeted kinase inhibitor therapy for acute myeloid leukemia. *Cancer cell*, 1(5):413–415, 2002.

[25] Mark Levis and Donald Small. Novel flt3 tyrosine kinase inhibitors. *Expert opinion on investigational drugs*, 12(12):1951–1962, 2003.

[26] Richard M Stone, Daniel J DeAngelo, Virginia Klimek, Ilene Galinsky, Eli Estey, Stephen D Nimer, Wilson Grandin, David Lebwohl, Yanfeng Wang, Pamela Cohen, Edward A. Fox, Donna Neuberg, Jennifer Clark, D. Gary Gilliland, and James D. Griffin. Patients with acute myeloid leukemia and an activating mutation in flt3 respond to a small-molecule flt3 tyrosine kinase inhibitor, pkc412. *Blood*, 105(1):54–60, 2005.

[27] Michael R Grunwald and Mark J Levis. Flt3 inhibitors for acute myeloid leukemia: a review of their efficacy and mechanisms of resistance. *International journal of hematology*, 97(6):683–694, 2013.

[28] Harinder Gill, Anskar YH Leung, and Yok-Lam Kwong. Molecularly targeted therapy in acute myeloid leukemia. *Future Oncology*, 12(6):827–838, 2016.

[29] Mona Hassanein, Muhamad H Almahayni, Syed O Ahmed, Sameh Gaballa, and Riad El Fakih. Flt3 inhibitors for treating acute myeloid leukemia. *Clinical Lymphoma Myeloma and Leukemia*, 16(10):543–549, 2016.

[30] Amir T Fathi and Yi-Bin Chen. The role of flt 3 inhibitors in the treatment of flt 3-mutated acute myeloid leukemia. *European journal of haematology*, 98(4):330–336, 2017.

This article is protected by copyright. All rights reserved.

Accepted Article

[31] Mark B Leick and Mark J Levis. The future of targeting flt3 activation in aml. *Current hematologic malignancy reports*, 12(3):153–167, 2017.

[32] Maria Larrosa-Garcia and Maria R Baer. Flt3 inhibitors in acute myeloid leukemia: current status and future directions. *Molecular cancer therapeutics*, 16(6):991–1001, 2017.

[33] Ran Friedman. Drug resistance in cancer: molecular evolution and compensatory proliferation. *Oncotarget*, 7(11):11746, 2016.

[34] Ellen Weisberg, Rosemary Barrett, Qingsong Liu, Richard Stone, Nathanael Gray, and James D Griffin. Flt3 inhibition and mechanisms of drug resistance in mutant flt3-positive aml. *Drug Resistance Updates*, 12(3):81–89, 2009.

[35] Nikolas von Bubnoff, Richard A Engh, Espen Åberg, Jana Sänger, Christian Peschel, and Justus Duyster. Fms-like tyrosine kinase 3–internal tandem duplication tyrosine kinase inhibitors display a nonoverlapping profile of resistance mutations in vitro. *Cancer research*, 69(7):3032–3041, 2009.

[36] E Weisberg, M Sattler, A Ray, and JD Griffin. Drug resistance in mutant flt3-positive aml. *Oncogene*, 29(37):5120, 2010.

[37] Mercedes E Gorre, Mansoor Mohammed, Katharine Ellwood, Nicholas Hsu, Ron Paquette, P Nagesh Rao, and Charles L Sawyers. Clinical resistance to sti-571 cancer therapy caused by bcr-abl gene mutation or amplification. *Science*, 293(5531):876–880, 2001.

[38] Ksenia Bagrintseva, Ruth Schwab, Tobias M Kohl, Susanne Schnittger, Sabine Eichenlaub, Joachim W Ellwart, Wolfgang Hiddemann, and Karsten Spiekermann. Mutations in the tyrosine kinase domain of flt3 define a new molecular mechanism of acquired drug resistance to ptk inhibitors in flt3-itd–transformed hematopoietic cells. *Blood*, 103(6):2266–2275, 2004.

[39] Florian Heidel, Fian K Solem, Frank Breitenbuecher, Daniel B Lipka, Stefan Kasper, MH Thiede, Christian Brandts, Hubert Serve, Johannes Roesel, Francis Giles, , Eric Feldman, Gerhard Ehninger, Gary J Schiller, Stephen Nimer, Richard M Stone, Yanfeng Wang, Thomas Kindler, Pamela S Cohen, Christoph Huber, and Thomas Fischer. Clinical resistance to the kinase inhibitor pkc412 in acute myeloid leukemia by mutation of asn-676 in the flt3 tyrosine kinase domain. *Blood*, 107(1):293–300, 2006.

[40] Carola Reindl, Ksenia Bagrintseva, Sridhar Vempati, Susanne Schnittger, Joachim W Ellwart, Katja Wenig, Karl-Peter Hopfner, Wolfgang Hiddemann, and Karsten Spiekermann. Point mutations in the juxtamembrane domain of flt3 define a new class of activating mutations in aml. *Blood*, 107(9):3700–3707, 2006.

[41] Rama Krishna Kancha, Rebekka Grundler, Christian Peschel, and Justus Duyster. Sensitivity toward sorafenib and sunitinib varies between different activating and drug-resistant flt3-itd mutations. *Experimental hematology*, 35(10):1522–1526, 2007.

[42] Catherine C Smith, Qi Wang, Chen-Shan Chin, Sara Salerno, Lauren E Damon, Mark J Levis, Alexander E Perl, Kevin J Travers, Susana Wang, Jeremy P Hunt, Patrick P Zarrinkar, Eric E Schadt, Andrew Kasarskis, John Kuriyan, and Neil P Shah. Validation of itd mutations in flt3 as a therapeutic target in human acute myeloid leukaemia. *Nature*, 485(7397):260, 2012.

[43] Catherine C Smith, Kimberly Lin, Adrian Stecula, Andrej Sali, and Neil P Shah. Flt3 d835 mutations confer differential resistance to type ii flt3 inhibitors. *Leukemia*, 29(12):2390, 2015.

[44] Chien-Cheng Lee, Yu-Chung Chuang, Yu-Lin Liu, and Chia-Ning Yang. A molecular dynamics simulation study for variant drug responses due to fms-like tyrosine kinase 3 g697r mutation. *RSC Advances*, 7(47):29871–29881, 2017.

[45] Qi Chao, Kelly G Sprankle, Robert M Grotzfeld, Andiliy G Lai, Todd A Carter, Anne Marie Velasco, Ruwanthi N Gunawardane, Merryl D Cramer, Michael F Gardner, Joyce James, Patrick P Zarrinkar, Hitesh K Patel, and Shripad S Bhagwat. Identification of n-(5-tert-butyl-isoxazol-3-yl)-n'-{4-[7-(2-morpholin-4-yl-ethoxy) imidazo [2, 1-b][1, 3] benzothiazol-2-yl] phenyl} urea dihydrochloride (ac220), a uniquely potent, selective, and efficacious fms-like tyrosine kinase-3 (flt3) inhibitor. *Journal of medicinal chemistry*, 52(23):7808–7816, 2009.

This article is protected by copyright. All rights reserved.

Accepted Article

[46] Patrick P Zarrinkar, Ruwanthi N Gunawardane, Merryl D Cramer, Michael F Gardner, Daniel Brigham, Barbara Belli, Mazen W Karaman, Keith W Pratz, Gabriel Pallares, Qi Chao, Kelly G Sprankle, Hitesh K Patel, Mark Levis, Robert C Armstrong, Joyce James, and Shripad S Bhagwat. Ac220 is a uniquely potent and selective inhibitor of flt3 for the treatment of acute myeloid leukemia (aml). *Blood*, 114(14):2984–2992, 2009.

[47] Daphnie Pauwels, Bram Sweron, and Jan Cools. The n676d and g697r mutations in the kinase domain of flt3 confer resistance to the inhibitor ac220. *Haematologica*, 97(11):1773, 2012.

[48] Catherine Choy Smith, Elisabeth A Lasater, Kimberly C Lin, Qi Wang, Melissa Quino McCreery, Whitney K Stewart, Lauren E Damon, Alexander E Perl, Grace R Jeschke, Mayumi Sugita, Martin Carroll, Scott C Kogan, John Kuriyan, and Neil P Shah. Crenolanib is a selective type i pan-flt3 inhibitor. *Proceedings of the National Academy of Sciences*, page 201320661, 2014.

[49] Catherine C Smith, Elisabeth A Lasater, Xiaotian Zhu, Kimberly C Lin, Whitney K Stewart, Lauren E Damon, Sara Salerno, and Neil P Shah. Activity of ponatinib against clinically-relevant ac220-resistant kinase domain mutants of flt3-itd. *Blood*, pages blood–2012, 2013.

[50] Catherine C Smith, Chao Zhang, Kimberly Lin, Elisabeth A Lasater, Ying Zhang, Evan Massi, Lauren E Damon, Matthew Pendleton, Ali Bashir, Robert P Sebra, Alexander E Perl, Andrew Kasarskis, Rafe Shellooe, Garson Tsang, Heidi Carias, Ben Powell, Elizabeth A Burton, Bernice Matusow, Jiazhong Zhang, Wayne Spevak, Prabha N Ibrahim, Mai H Le, Henry Hsu, Gaston G Habets, Brian L West, Gideon Bollag, and Neil P Shah. Characterizing and overriding the structural mechanism of the quizartinib-resistant flt3" gatekeeper" f691l mutation with plx3397. *Cancer discovery*, pages CD–15, 2015.

[51] G Todde and R Friedman. Activation and inactivation of the flt3 kinase: Pathway intermediates and the free energy of transition. *J. Phys. Chem. B*, In press:0, 2019.

[52] Morgan Huse and John Kuriyan. The conformational plasticity of protein kinases. *Cell*, 109(3):275–282, 2002.

[53] Lillian R Klug, Jason D Kent, and Michael C Heinrich. Structural and clinical consequences of activation loop mutations in class iii receptor tyrosine kinases. *Pharmacology & therapeutics*, 2018.

[54] Ketan S Gajiwala, Joe C Wu, James Christensen, Gayatri D Deshmukh, Wade Diehl, Jonathan P DiNitto, Jessie M English, Michael J Greig, You-Ai He, Suzanne L Jacques, Elizabeth A Lunney, Michele McTigue, David Molina, Terri Quenzer, Peter A Wells, Xiu Yu, Yan Zhang, Aihua Zou, Mark R Emmett, Alan G Marshall, Hui-Min Zhang, and George D Demetri. Kit kinase mutants show unique mechanisms of drug resistance to imatinib and sunitinib in gastrointestinal stromal tumor patients. *Proceedings of the National Academy of Sciences*, 106(5):1542–1547, 2009.

[55] Jonathan P DiNitto, Gayatri D Deshmukh, Yan Zhang, Suzanne L Jacques, Rocco Coli, Joseph W Worrall, Wade Diehl, Jessie M English, and Joe C Wu. Function of activation loop tyrosine phosphorylation in the mechanism of c-kit auto-activation and its implication in sunitinib resistance. *The journal of biochemistry*, 147(4):601–609, 2010.

[56] Yesid Alvarado, Hagop M Kantarjian, Rajyalakshmi Luthra, Farhad Ravandi, Gautam Borthakur, Guillermo Garcia-Manero, Marina Konopleva, Zeev Estrov, Michael Andreeff, and Jorge E Cortes. Treatment with flt3 inhibitor in patients with flt3-mutated acute myeloid leukemia is associated with development of secondary flt3–tyrosine kinase domain mutations. *Cancer*, 120(14):2142–2149, 2014.

[57] Ran Friedman. The molecular mechanism behind resistance of the kinase flt3 to the inhibitor quizartinib. *Proteins: Structure, Function, and Bioinformatics*, 85(11):2143–2152, 2017.

[58] Matthew A Young, Neil P Shah, Luke H Chao, Markus Seeliger, Zdravko V Milanov, William H Biggs, Daniel K Treiber, Hitesh K Patel, Patrick P Zarrinkar, David J Lockhart, Charles L Sawyers, and John Kuriyan. Structure of the kinase domain of an imatinib-resistant abl mutant in complex with the aurora kinase inhibitor vx-680. *Cancer research*, 66(2):1007–1014, 2006.

Accepted Article

This article is protected by copyright. All rights reserved.

[59] Julie A Zorn, Qi Wang, Eric Fujimura, Tiago Barros, and John Kuriyan. Crystal structure of the flt3 kinase domain bound to the inhibitor quizartinib (ac220). *PloS one*, 10(4):e0121177, 2015.

[60] Markus A Seeliger, Matthew Young, M Nidanie Henderson, Patricia Pellicena, David S King, Arnold M Falick, and John Kuriyan. High yield bacterial expression of active c-abl and c-src tyrosine kinases. *Protein Science*, 14(12):3135–3139, 2005.

[61] A Goldenzweig, Me Goldsmith, SE Hill, O Gertman, P Laurino, Y Ashani, O Dym, T Unger, S Albeck, J Prilusky, RL Lieberman, A Aharoni, I Silman, JL Sussman, DS Tawfik, and SJ Fleishman. Automated structure-and sequence-based design of proteins for high bacterial expression and stability. *Molecular cell*, 63(2):337–346, 2016.

[62] Jeffrey H Till, Ararat J Ablooglu, Mark Frankel, Steven M Bishop, Ronald A Kohanski, and Stevan R Hubbard. Crystallographic and solution studies of an activation loop mutant of the insulin receptor tyrosine kinase insights into kinase mechanism. *Journal of Biological Chemistry*, 276(13):10049–10055, 2001.

[63] Jonah Beenstock, Navit Mooshayef, and David Engelberg. How do protein kinases take a selfie (autophosphorylate)? *Trends in biochemical sciences*, 41(11):938–953, 2016.

[64] Shruti Agarwal, Julhash U Kazi, and Lars Rönnstrand. Phosphorylation of the activation loop tyrosine 823 in c-kit is crucial for cell survival and proliferation. *Journal of Biological Chemistry*, pages jbc–M113, 2013.

[65] Thomas Schindler, William Bornmann, Patricia Pellicena, W Todd Miller, Bayard Clarkson, and John Kuriyan. Structural mechanism for sti-571 inhibition of abelson tyrosine kinase. *Science*, 289(5486):1938–1942, 2000.

[66] Julhash U Kazi, Rohit A Chougule, Tianfeng Li, Xianwei Su, Sausan A Moharram, Kaja Rupar, Alissa Marhäll, Mohiuddin Gazi, Jianmin Sun, Hui Zhao, and Lars Rönnstrand. Tyrosine 842 in the activation loop is required for full transformation by the oncogenic mutant flt3-itd. *Cellular and Molecular Life Sciences*, 74(14):2679–2688, 2017.

[67] R Friedman, K Boye, and K Flatmark. Molecular modelling and simulations in cancer research. *Biochim Biophys Acta*, 1836:1–14, 2013.

[68] Panagiota S Georgoulia, Guido Todde, Sinisa Bjelic, and Ran Friedman. The catalytic activity of abl1 single and compound mutations: Implications for the mechanism of drug resistance mutations in chronic myeloid leukaemia. *Biochimica et Biophysica Acta (BBA)-General Subjects*, 1863(4):732–741, 2019.

[69] I. Echeverria, Y. Liu, S. B. Gabelli, and L. M. Amzel. Oncogenic mutations weaken the interactions that stabilize the p110α-p85α heterodimer in phosphatidylinositol 3-kinase α. *FEBS J.*, 282(18):3528–3542, Sep 2015.

[70] H. Leontiadou, I. Galdadas, C. Athanasiou, and Z. Cournia. Insights into the mechanism of the PIK3CA E545K activating mutation using MD simulations. *Sci Rep*, 8(1):15544, Oct 2018.

[71] Andrej Šali and Tom L Blundell. Comparative protein modelling by satisfaction of spatial restraints. *Journal of molecular biology*, 234(3):779–815, 1993.

[72] William D Tap, Zev A Wainberg, Stephen P Anthony, Prabha N Ibrahim, Chao Zhang, John H Healey, Bartosz Chmielowski, Arthur P Staddon, Allen Lee Cohn, Geoffrey I Shapiro, , VL Keedy, AS Singh, I Puzanov, EL Kwak, Wagner AJ, DD Von Hoff, GJ Weiss, RK Ramanathan, J Zhang, G Habets, Y Zhang, EA Burton, G Visor, L Sanftner, P Severson, H Nguyen, MJ Kim, A Marimuthu, G Tsang, R Shellooe, C Gee, BL West, P Hirth, K Nolop, M van de Rijn, HH Hsu, C Peterfy, PS Lin, S Tong-Starksen, and G Bollag. Structure-guided blockade of csf1r kinase in tenosynovial giant-cell tumor. *New England Journal of Medicine*, 373(5):428–437, 2015.

[73] Vincent Zoete, Michel A Cuendet, Aurélien Grosdidier, and Olivier Michielin. Swissparam: a fast force field generation tool for small organic molecules. *Journal of computational chemistry*, 32(11):2359–2368, 2011.

[74] Eric F Pettersen, Thomas D Goddard, Conrad C Huang, Gregory S Couch, Daniel M Greenblatt, Elaine C Meng, and Thomas E Ferrin. Ucsf chimera—a visualization system for exploratory research and analysis. *Journal of computational chemistry*, 25(13):1605–1612, 2004.

This article is protected by copyright. All rights reserved.

Accepted Article

[75] Julie D Thompson, Toby J Gibson, and Des G Higgins. Multiple sequence alignment using clustalw and clustalx. *Current protocols in bioinformatics*, 00(1):2.3.1–2.3.22, 2003.

[76] Kazutaka Katoh, Kazuharu Misawa, Kei-ichi Kuma, and Takashi Miyata. Mafft: a novel method for rapid multiple sequence alignment based on fast fourier transform. *Nucleic acids research*, 30(14):3059–3066, 2002.

[77] H J C Berendsen, D van der Spoel, and R Vandrunen. Gromacs-a Message-Passing Parallel Molecular-Dynamics Implementation. *Comput. Phys. Commun.*, 91:43–56, 1995.

[78] D van der Spoel, E Lindhal, B Hess, G Groenhof, A E Mark, and H J C Berendsen. GROMACS: Fast, Flexible, and Free. *J. Comput. Chem.*, 26:1701–1718, 2005.

[79] Alexander D MacKerell Jr, Donald Bashford, MLDR Bellott, Roland Leslie Dunbrack Jr, Jeffrey D Evanseck, Martin J Field, Stefan Fischer, Jiali Gao, H Guo, Sookhee Ha, D Joseph-McCarthy, L Kuchni, K Kuczera, F T K Lau, C Mattos, S Michnick, T Ngo, D T Nguyen, B Prodhom, W E Reiher, B Roux, M Schlenkrich, J C Smith, R Stote, J Straub, M Watanabe, J Wiórkiewicz-Kuczera, D Yin, and Karplus M. All-atom empirical potential for molecular modeling and dynamics studies of proteins. *The journal of physical chemistry B*, 102(18):3586–3616, 1998.

[80] Alexander D MacKerell Jr. Empirical force fields for biological macromolecules: overview and issues. *Journal of computational chemistry*, 25(13):1584–1604, 2004.

[81] W L Jorgensen, J Chandrasekhar, J D Madura, R W Impey, and M L Klein. Comparison of Simple Potential Funtions for Simulating Liquid Water. *J. Chem. Phys.*, 79:926–935, 1983.

[82] G Bussi, D Donadio, and M Parrinello. Canonical Sampling through Velocity-Rescaling. *J. Chem. Phys.*, 126:014101, 2007.

[83] H. J. C. Berendsen, J. P. M. Postma, A. DiNola, and J. R. Haak. Molecular dynamics with coupling to an external bath. *J. Chem. Phys.*, 81:3684–90, 1984.

[84] M Parrinello and A Rahman. Polymorphic Transitions in Single Crystals: a New Molecular Dynamics Method. *J. Appl. Phys.*, 52:7182–7190, 1981.

[85] T Darden, D York, and L Pedersen. Particle Mesh Ewald: an N·log(N) Method ofr Ewald Sums in Large Systems. *J. Chem. Phys.*, 98:10089–10092, 1993.

[86] U Essmann, L Perera, M L Berkowitz, T Darden, H Lee, and L G Pedersen. A Smooth Particle Mesh Ewald Method. *J. Chem. Phys.*, 103:8577–8593, 1995.

[87] B Hess, H Bekker, H J C Berendsen, and J G E M Fraaije. LINCS: a Linear Constraint Solver for Molecular Simualtions. *J. Comput. Chem.*, 18:1463–1472, 1997.

[88] S. Miyamoto and P. A. Kollman. SETTLE: An analytical version of the SHAKE and RATTLE algorithms for rigid water models. *J. Comp. Chem.*, 13:952–962, 1992.

[89] Nicholas M Glykos. Software news and updates carma: A molecular dynamics analysis program. *Journal of computational chemistry*, 27(14):1765–1768, 2006.

[90] Warren L DeLano. The pymol molecular graphics system. *http://www. pymol. org*, 2002.

[91] Barry J Grant, Ana PC Rodrigues, Karim M ElSawy, J Andrew McCammon, and Leo SD Caves. Bio3d: an r package for the comparative analysis of protein structures. *Bioinformatics*, 22(21):2695–2696, 2006.

[92] A Leaver-Fay, M Tyka, Lewis. SM, OF Lange, J Thompson, R Jacak, K Kaufman, PD Renfrew, CA Smith, W Sheffler, IW Davis, S Cooper, A Treuille, DJ Mandell, F Richter, YE Ban, SJ Fleishman, JE Corn, DE Kim, S Lyskov, M Berrondo, S Mentzer, Z Popovic, JJ Havranek, J Karanicolas, R Das, J Meiler, T Kortemme, JJ Gray, B Kuhlman, D Baker, and P Bradley. Rosetta3: an object-oriented software suite for the simulation and design of macromolecules. In *Methods in enzymology*, volume 487, pages 545–574. Elsevier, 2011.

This article is protected by copyright. All rights reserved.

Accepted Article

[93] T A Kunkel. Rapid and Efficient Site-Specific Mutagenesis without Phenotypic Selection. *Proc. Natl. Acad. Sci. U.S.A.*, 82:488–492, 1985.

Accepted Article

This article is protected by copyright. All rights reserved.

FIGURE 1 FLT3-KD drugs and conformations. (A) FLT3-KD in inactive (**PDB ID 4RT7** [50]) and active states (model). Residues at drug resistance mutation sites (M664, D835, Y842) and the gate-keeper F691 are illustrated in stick orange colour representation. The main structural kinase features are highlighted in different colours. (B) Chemical structure of quizartinib and PLX3397. Both drugs target the ATP binding site in the inactive conformation (type II inhibitors).

FIGURE 2 Occupancy of protein-drug interactions. The interactions between protein residues and PLX3397 or quizartinib that were calculated over the simulation time, are represented for the native FLT3-KD and the mutants. The colour scale from white to blue follows the observed frequency of the contacts (defined by a distance cut-off of 4Å between heavy atoms of the protein and the drug). (A) Colour-matrix representation of all calculated protein-drug interactions. Protein residues of FLT3-KD that have been documented as drug resistance mutation sites are marked with a red arrow. (B) Representation of the interactions in a structural content for the native FLT3-KD and each drug (green colour). Each drug-interacting protein residue is shown in stick representation, using the same colour scale to highlight the impact on the dynamics of the protein-drug interactions. Drug-resistance residue sites i.e., F691, G697 and D698 are also depicted. The complete set is presented in Figure 3.

FIGURE 3 Protein-drug interactions. The interactions between protein residues and PLX3397 or quizartinib that were calculated over the simulation time, are represented for the native FLT3-KD and the mutants. Each drug-interacting protein residue is shown in stick representation and coloured from white to blue according to the frequency of the interaction with the drug (green colour). F691, G697 and D698 are known drug-resistance mutation sites. D835N and M664I are the drug-resistance mutations under study (Y842S is further away and omitted in the representation).

FIGURE 4 Principle component analysis based clustering. Clustering of conformations observed during each cumulative 1μs trajectory. The main cluster is coloured blue and the others are coloured in greyscale. The size of the bar is representative of the occupancy of the cluster (calculated over the total cluster-assigned frames, the number of which was similar in all 16 systems). The projections of trajectories on the principal components is presented in Figure 5. PCA and corresponding cluster analysis were performed with CARMA[89].

FIGURE 5 Density distributions of the first two principal components from a PCA analysis in dihedral space. Each diagram is a density representation (with yellow-red colours representing high densities) of the projection of each trajectory on the plane defined by the first (x-axis) and second (y-axis) eigenvector from a dihedral principal component analysis. The cluster analysis presented in Figure 4 was performed using the top 5 principal components. The variance explained by the clustering procedure is shown on the bottom right of each sub-figure. PCA and corresponding cluster analysis were performed with CARMA[89].

FIGURE 6 Difference frequency-contact maps. Contacts between residues that were formed or broken during simulations were compared and represented with the coloured lines on the kinase structure. (A) comparison between inactive and +PLX3397 native trajectories, (B) comparison between inactive and +quizartinib native trajectories, (C) comparison between +PLX3397 and +quizartinib native trajectories, (D) comparison between inactive and active KD-M664I trajectories, (E) comparison between inactive and +quizartinib KD-Y842S trajectories. Drug resistance mutations for PLX3397 and quizartinib are annotated in panels A and B, respectively. Warm colours (yellow to red) are used for contacts observed with higher frequency in the first trajectory under comparison and cold colours (cyan to blue) are used for contacts observed with higher frequency in the second trajectory with red and blue representing contacts observed only in the first or second trajectory, respectively. The width of each line is proportional to the calculated frequency of the contact. The complete set of comparisons is presented in Figure 7.

This article is protected by copyright. All rights reserved.

Accepted Article

FIGURE 7 Difference frequency-contact maps. Contacts between residues that were formed or broken during simulations are compared and represented with the coloured lines on the kinase structure. Each row shows a comparison between the native sequence and each mutant (one per column), in the inactive, active, +PLX3397, +quizartinib trajectories. Warm colours (yellow to red) are used for contacts observed with higher frequency in the native trajectory and cold colours (cyan to blue) are used for contacts observed with higher frequency in the trajectory under comparison with red and blue representing contacts observed only in the first or second trajectory, respectively. The width of each line is proportional to the calculated frequency of the contact.

FIGURE 8 FLT3 kinase domain activity. (A) Sites of solubilising mutations predicted by the PROSS server [61]. The native KD is coloured red and the designed KD is coloured cyan. Individual surface residues that were chosen to be mutated in the design are labelled and shown in stick representation. (B) Coomassie blue stained SDS-PAGE gel analysis of FLT3-KD design protein two-step purification scheme showing elution fractions from affinity chromatography step (1) and size-exclusion chromatography (SEC) step (2). (C) SEC elution profiles of FLT3-KD design and mutants. All proteins appear monomeric with elution volumes corresponding to molecular weights of 41-45kDa (the predicted molecular weight is 41.7kDa). (D) Phosphorylation activity for the substrate (MBP protein) for the native KD, the design and the drug resistant mutants M664I, D835N, Y842S. (E) Autophosphorylation activity (without MBP protein) for the same set of proteins. Average activity values and standard deviations (error bars) were calculated over two experiments, each of which was performed in triplicates. The comparison between average values was performed with one-way ANOVA followed by post hoc Tukey test to estimate the level of statistical significance of the differences (ns = $P > 0.05$, $* = P \leq 0.05$, $** = P \leq 0.01$, $*** = P \leq 0.001$).

FIGURE 9 Stereo view of the structural superposition between quizartinib (white colour) and PLX3397 (gray colour). For clarity only protein residues within 4Å of the drug are shown in stick representation and the rest of the structure in transparent cartoon representation (orange colour for FLT3-KD, **PDB ID 4rt7** and yellow colour for CSF-1-R-KD, **PDB ID 4r7h**). Note that the depicted clash concerns the drug quizartinib and a tryptophan residue from the other protein, CSF-1-R.

FIGURE 10 UPGMA (unweighted pair group method with arithmetic mean) tree of the MSA (multiple sequence alignment) of kinases with crystallographically determined active conformations. The 22 kinases clustered together (red branches) and closest to the sequence of FLT3-KD (highlighted yellow) were used as templates to built a model of the active conformation of FLT3-KD, shown in Figure 1. MSA was calculated with ClustalW [75] and UPGMA tree was constructed with MAFFT [76].

FIGURE 11 Comparison of simulations of native and design FLT3-KD. (A) Histogram distribution of the RMSD values calculated between each structure in the design simulation (design, design M664I) and the closest structure found in the native simulation (native, M664I) for both inactive and active conformations. (B) Histogram distribution of the RMSD values calculated between all clustered structures in each design simulation to all clustered structures in the corresponding native simulation. (C) PCA-based clustering, as presented in Figure 3. (D Density distributions of the first two principal components from a PCA analysis in dihedral space, as presented in Figure 5. For comparison purposes, in (C) and (D) the results for the native systems (native, M664I) are included.

This article is protected by copyright. All rights reserved.

Accepted Article

Acknowledgements

This work was supported by the Swedish Cancer Society (Cancerfonden), project number CAN 2015/387 to RF; and by the Crafoord Foundation, project number 20160653 to SB.

Author contributions

PSG performed the experiments and simulations. All authors designed the study and wrote the article.

Conflicts of Interest

The authors declare not competing interests.

Accepted Article

This article is protected by copyright. All rights reserved.

Graphical Abstract

FLT3 is a kinase that is an important drug target in leukaemias, but resistance to therapies directed at FLT3 occurs often due to mutations. We used enzymatic experiments and computer simulations to study how mutations lead to resistance, and found that the main effect is increased activity which is explained by structural and dynamic changes to the active conformation.

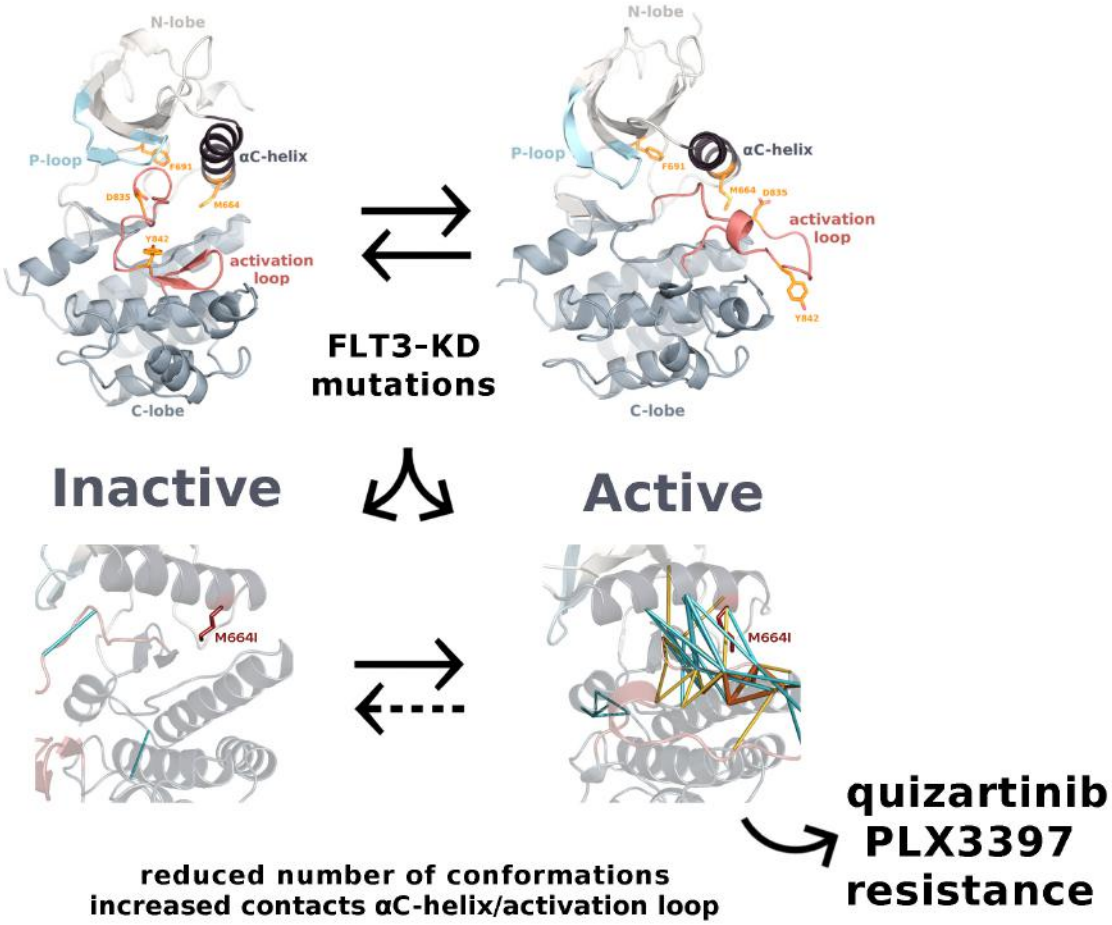

This article is protected by copyright. All rights reserved.

Figure 1

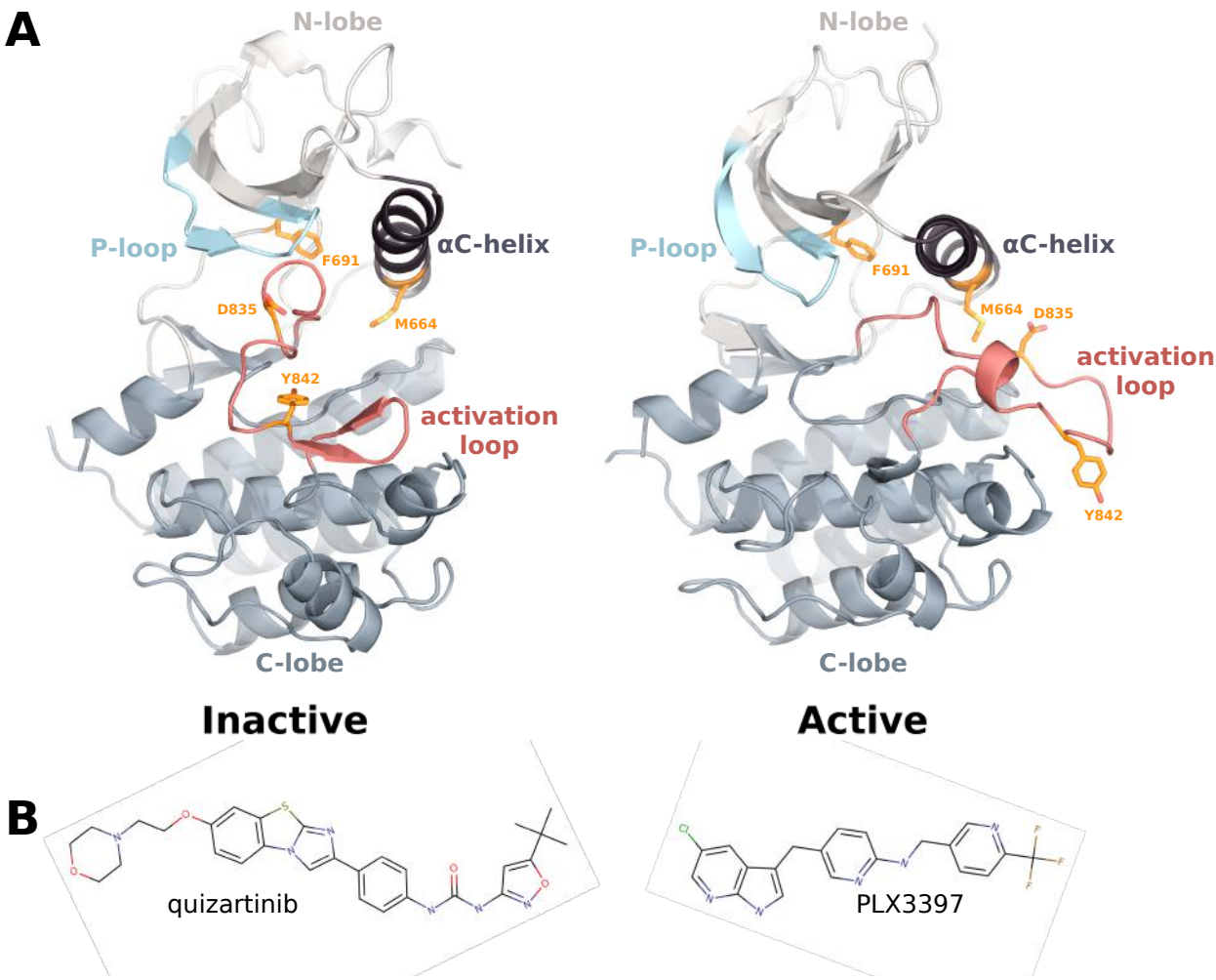

This article is protected by copyright. All rights reserved.

Figure 2

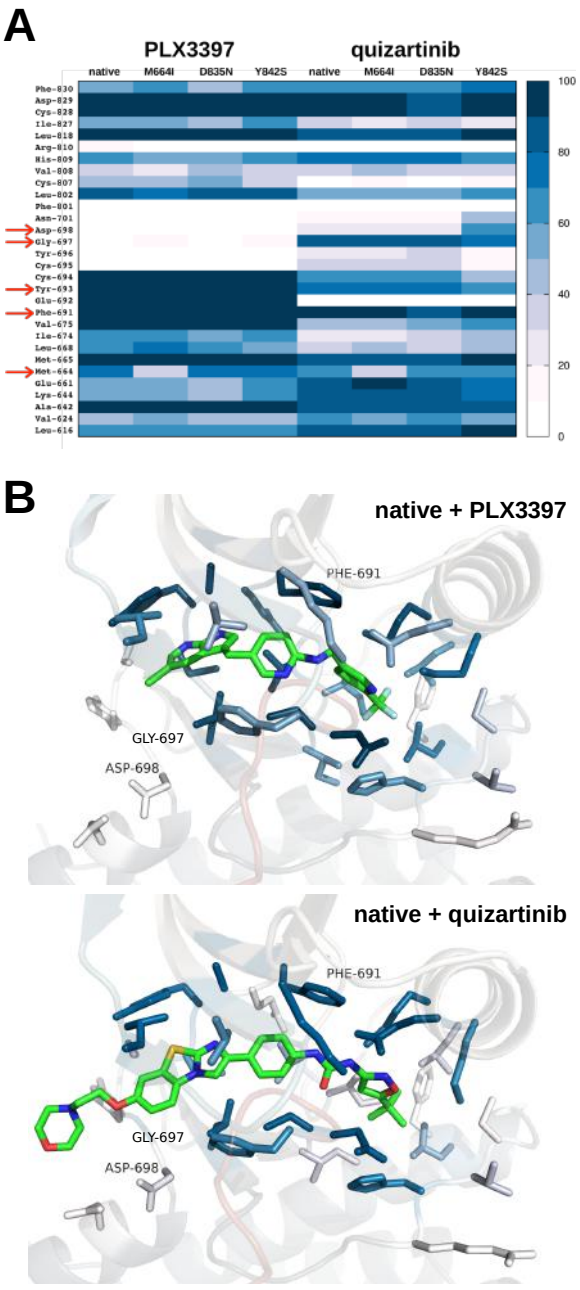

This article is protected by copyright. All rights reserved.

Figure 3

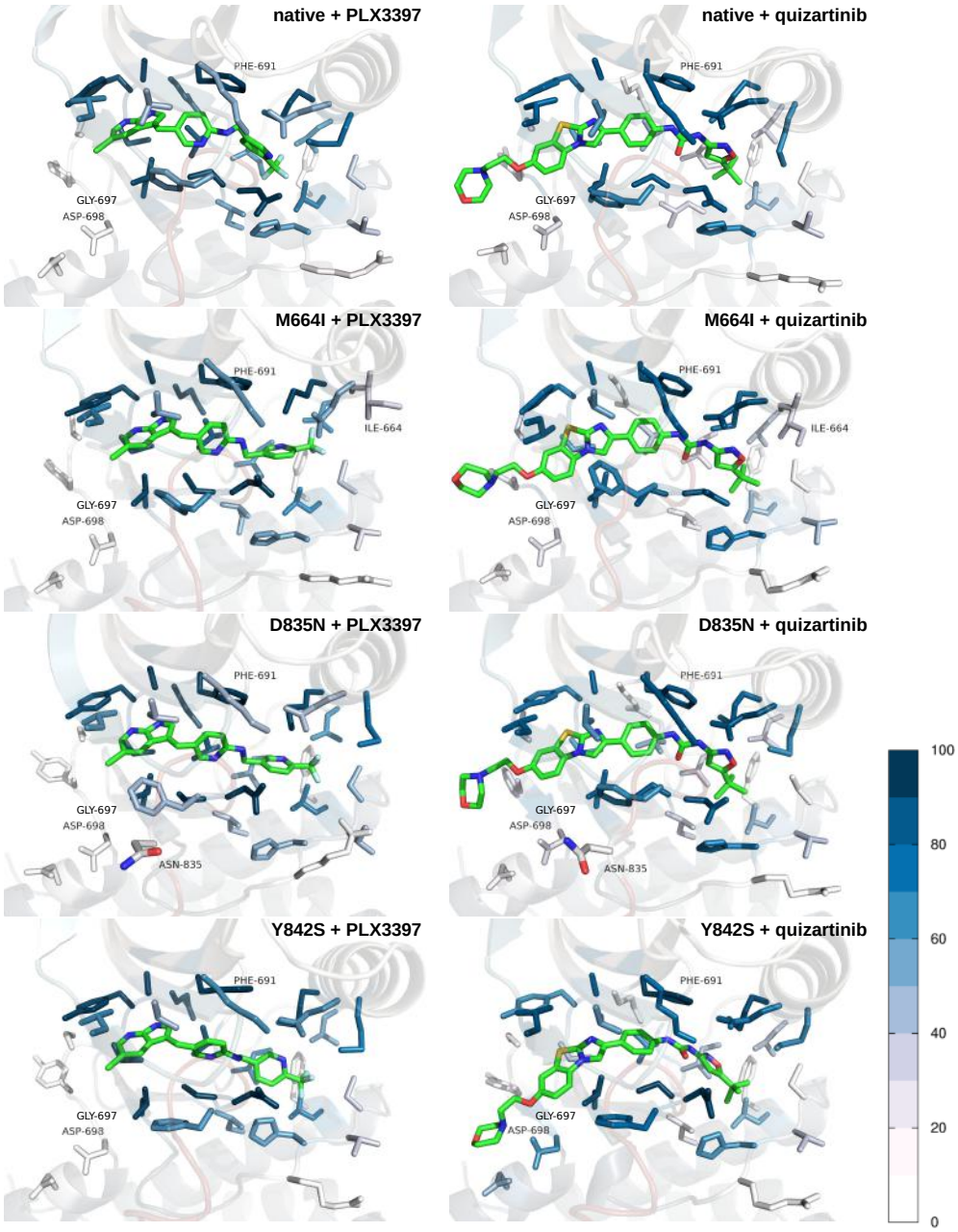

This article is protected by copyright. All rights reserved.

Figure 4

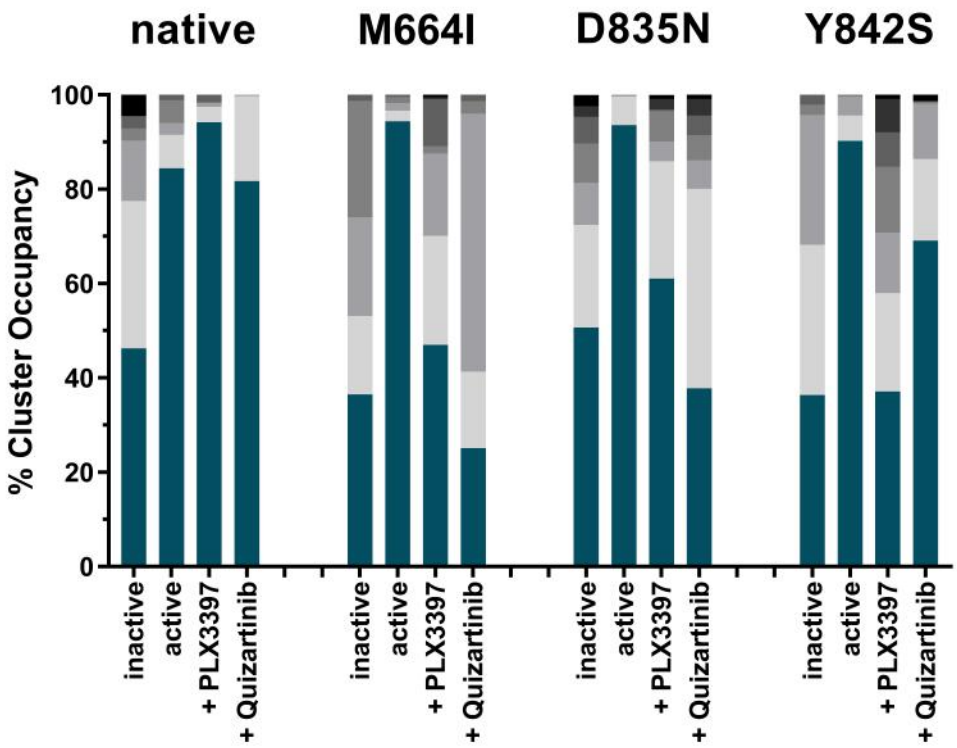

This article is protected by copyright. All rights reserved.

Figure 5

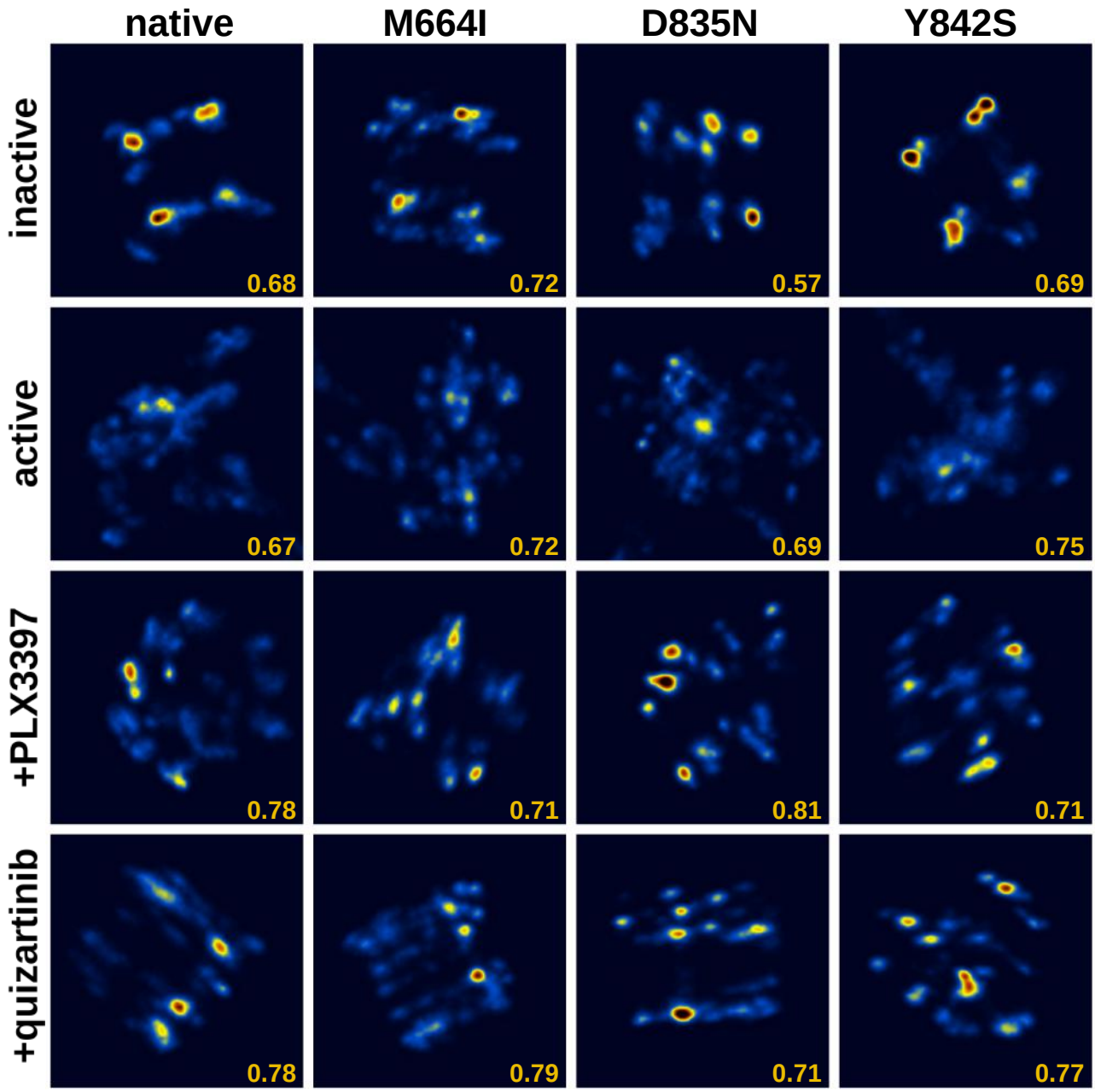

This article is protected by copyright. All rights reserved.

Figure 6

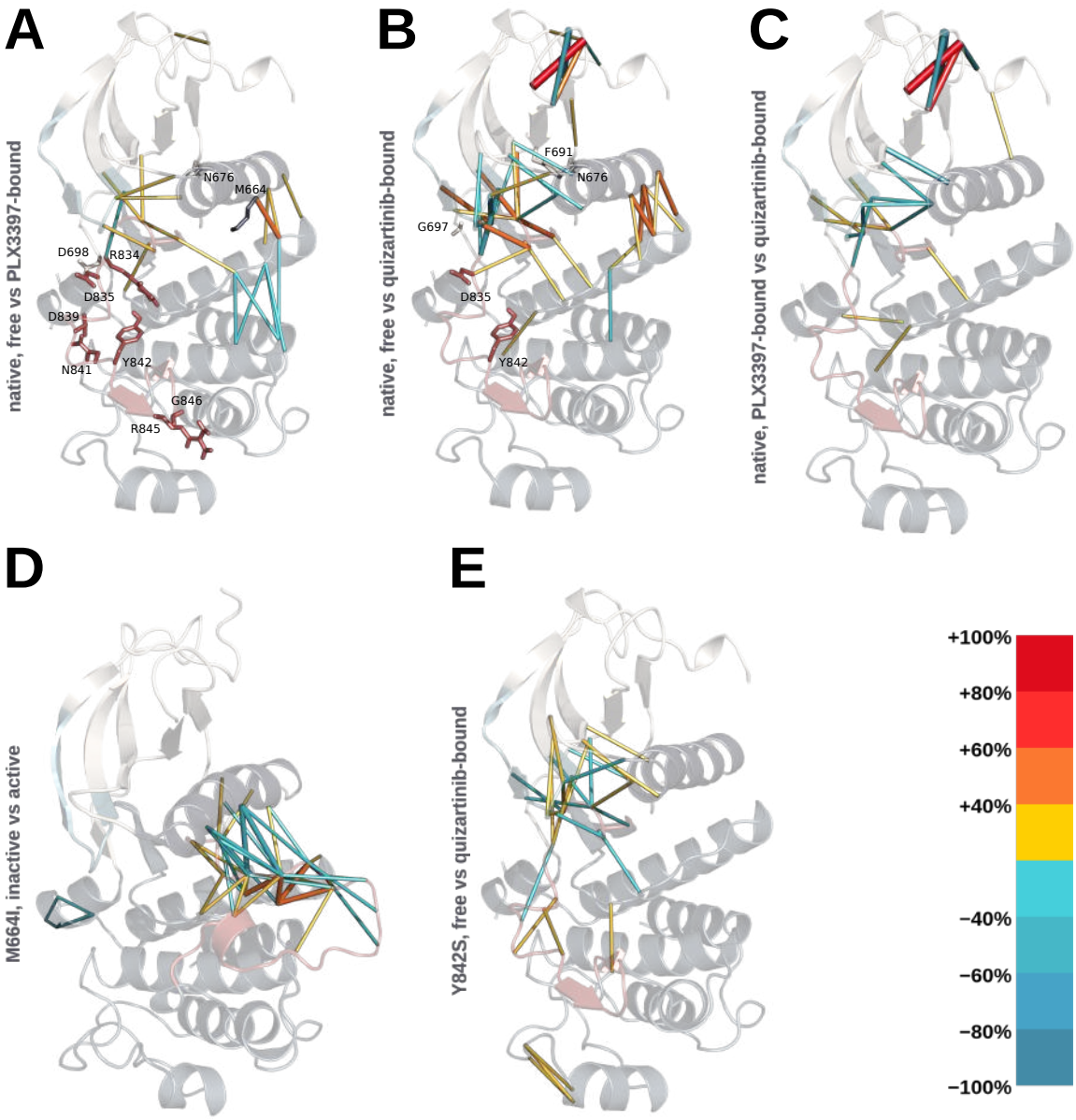

This article is protected by copyright. All rights reserved.

Figure 7

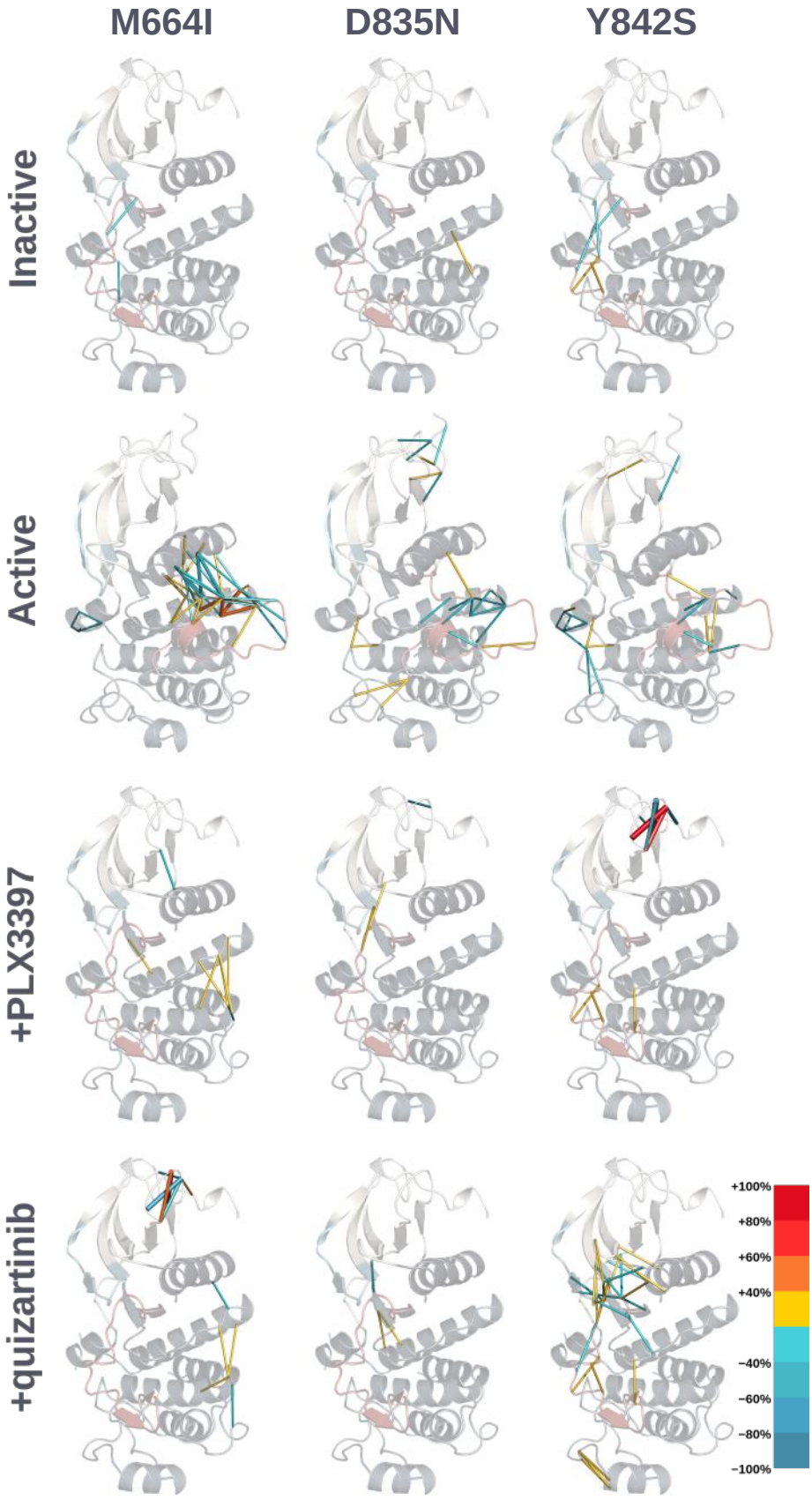

This article is protected by copyright. All rights reserved.

Figure 8

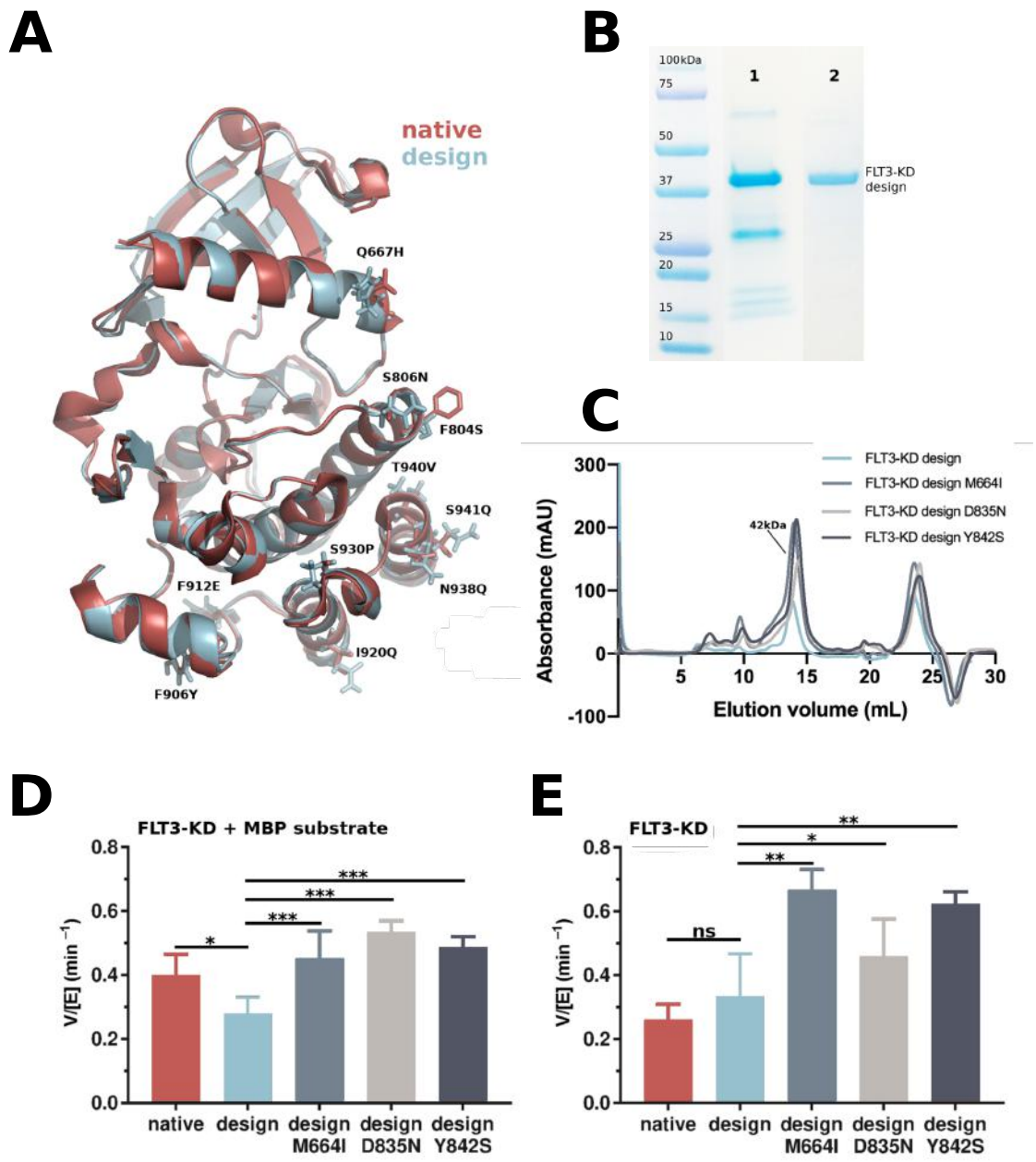

This article is protected by copyright. All rights reserved.

Figure 9

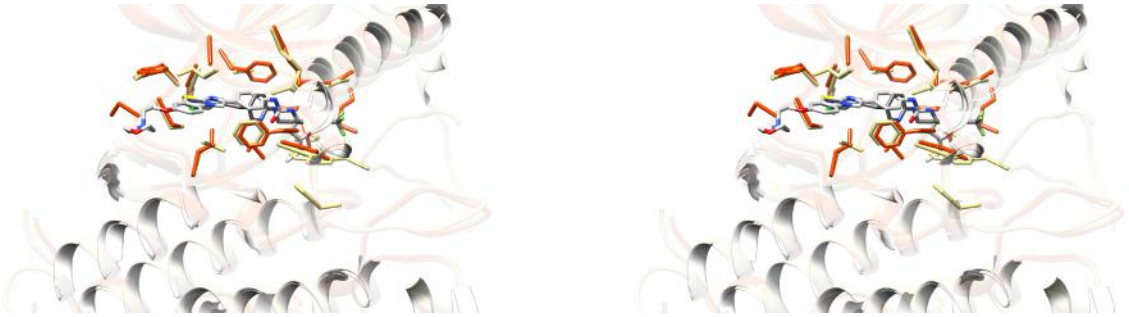

This article is protected by copyright. All rights reserved.

Figure 10

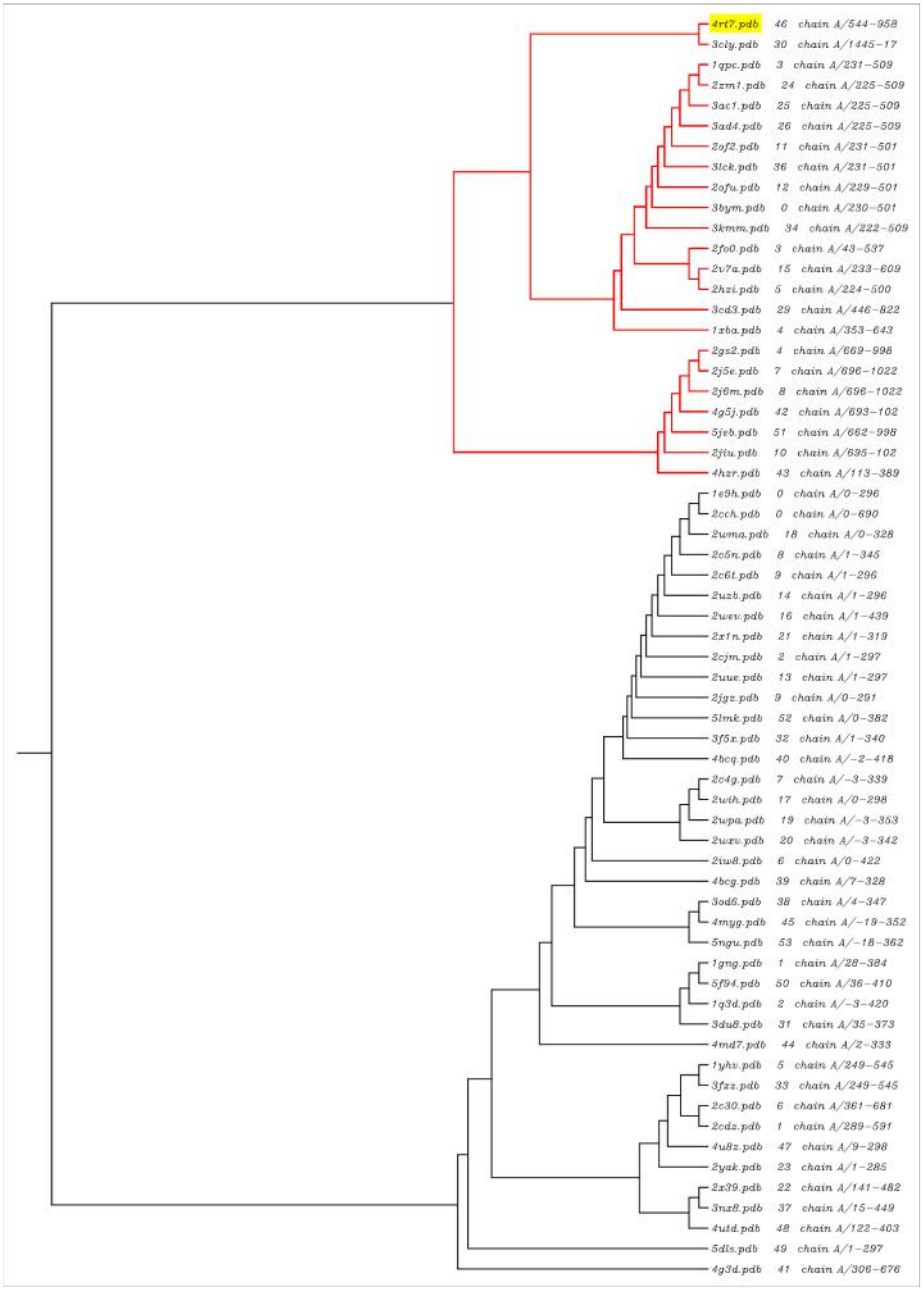

This article is protected by copyright. All rights reserved.

Figure 11

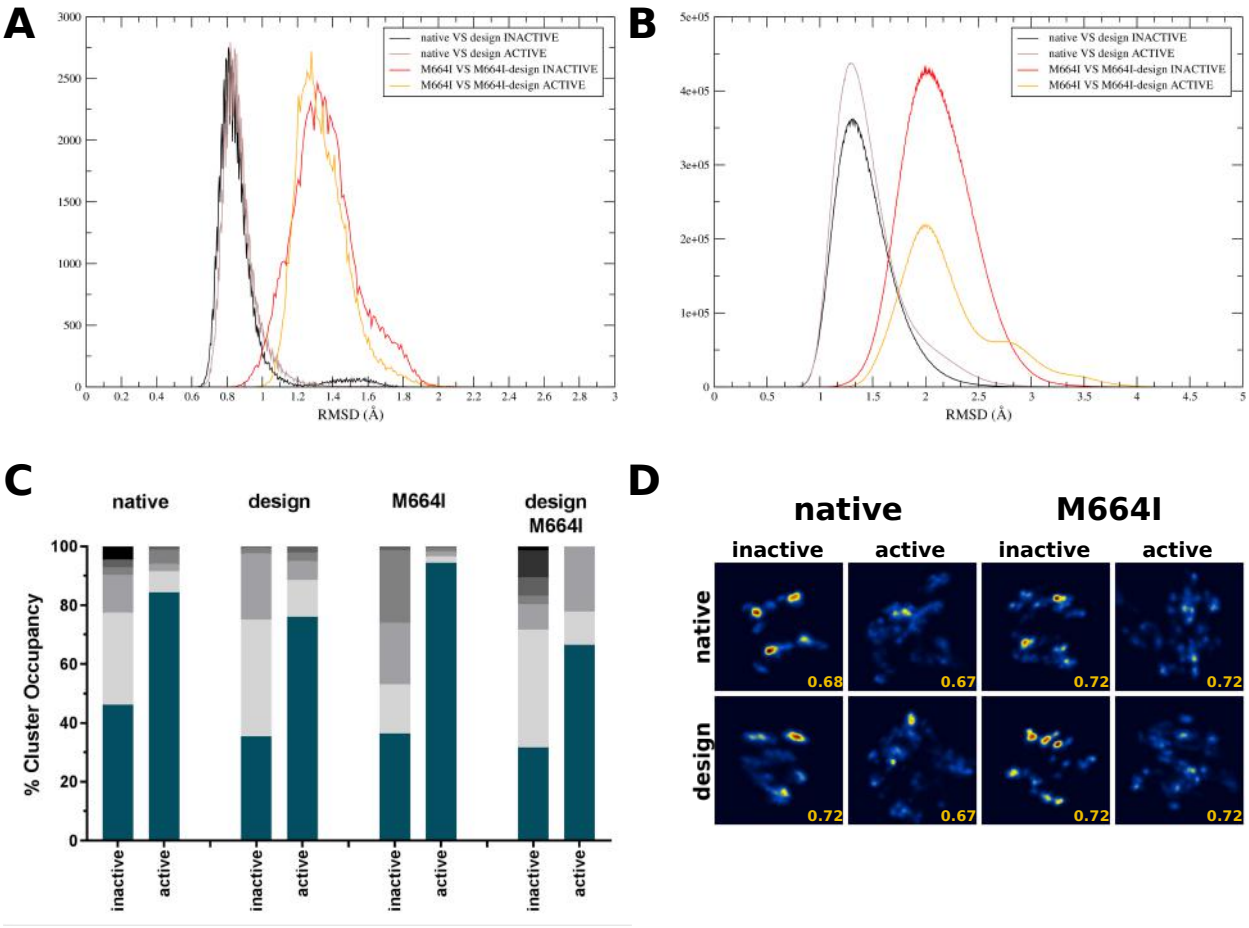

This article is protected by copyright. All rights reserved.